

Elsevier Editorial System(tm) for Ocean & Coastal Management
Manuscript Draft

Manuscript Number: OCMA-D-14-00135R1

Title: Temporal evolution of patterns and processes related to subsidence of the coastal area surrounding the Bevano River Mouth (Northern Adriatic) - Italy

Article Type: SI: ECSA53

Keywords: Subsidence, Coastal Areas, Remote Sensing, Permanent Scatter, Monitoring, Underground water, Vegetation.

Corresponding Author: Prof. Andrea Taramelli, PhD

Corresponding Author's Institution: ISPRA

First Author: Andrea Taramelli, PhD

Order of Authors: Andrea Taramelli, PhD; Lucio Dimatteo, PhD; Paolo Ciavola, PhD; Fabio Guadagnano, BSC; Cristiano Tolomei, MSC

Manuscript Region of Origin: ITALY

- Temporal evolution of patterns and processes on a stretch of coast
- Multi-temporal analysis of processes and trends related to subsidence in coastal landscapes.
- Marshlands reclamation, groundwater pumping and methane extraction from gas fields are the main anthropogenic causes.

Temporal evolution of patterns and processes related to subsidence of the coastal area surrounding the Bevano River Mouth (Northern Adriatic) – Italy

A. Taramelli¹, L. Di Matteo², P. Ciavola³, F. Guadagnano², C. Tolomei⁴

Andrea Taramelli PhD, ISPRA Institute for Environmental Protection and Research, via Vitaliano Brancati, 60, Rome, Italy, Office: +39-06-5007-4635 - Fax: +39-06-5007-4912, andrea.taramelli@isprambiente.it

Lucio Di Matteo (PhD), Earth Sciences Department, University of Perugia, 06123 - Perugia (Italy), Tel. +39 0755849694, Fax. +39 0755840302 - lucio.dimatteo@unipg.it webpage: <http://accounts.unipg.it/~dimatteo>

Paolo Ciavola, Associate Professor of Coastal Dynamics and Geohazards, Dipartimento di Fisica e Scienze della Terra, Università di Ferrara, Ferrara, Italy, Tel. +39-0532974622, e-mail: cvp@unife.it

Fabio Guadagnano, Dipartimento di Fisica e Geologia, Università degli Studi di Perugia, Via Alessandro Pascoli s.n.c., Perugia, Italia.

Dr. Cristiano Tolomei, Remote Sensing Laboratory, Istituto Nazionale di Geofisica e Vulcanologia, Via di Vigna Murata, 605, 00143 Rome, ITALY, Tel : ++ 39 06 51860384, Fax : ++ 39 06 51860541, e-mail: [mailto: tolomei@ingv.it](mailto:tolomei@ingv.it) - INGV Web Site: <http://www.ingv.it>



ISPRA

Istituto Superiore per la Protezione
e la Ricerca Ambientale

Roma, 28/03/14

Subject: Submission of a research papers

With regard to the manuscript:

Temporal evolution of patterns and processes related to subsidence of the coastal area surrounding the Bevano River Mouth (Northern Adriatic) – Italy

A. Taramelli¹, L. Di Matteo², P. Ciavola³, F. Guadagnano², C. Tolomei⁴

[1] ISPRA Istituto Superiore Protezione e Ricerca Ambientale, Via Vitaliano Brancati, 48, Roma, Italia.

[2] Dipartimento di Fisica e Geologia, Università degli Studi di Perugia, Via Alessandro Pascoli s.n.c., Perugia, Italia.

[3] Dipartimento di Fisica e Scienze della Terra, Università degli Studi di Ferrara, Via Saragat, 1, Ferrara, Italia.

[4] INGV Istituto Nazionale di Geofisica e Vulcanologia, Via di Vigna Murata, 605, Roma, Italia.

*** Corresponding author: andrea.taramelli@isprambiente.it**

While planning coastal risk management strategies, coastal managers need to assess risk across a range of spatial and temporal scales. Space borne based tools are one efficient way to support them in the decision making process through a scenarios analysis starting from economic and environmental information integrated into a common platform. However, this integration process requires a significant effort from a team of scientists in terms of a) identifying the appropriate scales and data resolution for analysing environmental and economic issues; b) selecting and linking an appropriate set of tools to build a coupled model; c) developing space-borne criteria analysis to integrate environmental and economic impacts; and e) accounting for the expectations of the stakeholders and therefore optimizing the opportunity for them to interact with the tool development and with the final tool itself.

The present paper was developed under the European Commission funding schem through the project “Innovative Technologies for safer European coasts in a changing climate” (THESEUS), Contract 244104, FP7.2009-1, www.theseusproject.eu.

The paper represent a 4 year research to characterized the complex interactions between morphology and biota in a small estuary through the implementation of different algorithms on multispectral endmember fraction maps from optical space-borne remote

sensing. Multitemporal fractional abundance maps spanning from 1986 to 2011 were used to identify the interaction between vegetation pattern dynamics and other physical parameters like subsidence rate. The objectives were to: a) analyze and validate the processing procedure used to define the patterns; b) support the classification of the different surface types for the development of new methods for monitoring coastal systems.

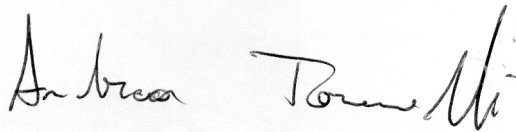
This manuscript describes original work and is not under consideration by any other journal. All authors approved the manuscript and this submission.

Thank you in advance for giving the possibility of submitting our manuscript and considering it for review.

Looking forward to your response, my (and ours) best regards,

We look forward to hear back from you soon.

Best Regards,
Andrea Taramelli

A handwritten signature in black ink, reading "Andrea Taramelli". The signature is written in a cursive style with a large initial 'A' and 'T'.

1 **Abstract**

2 Subsidence is a widespread phenomenon in the Emilia-Romagna, particularly important along the
3 littoral because the coastal system consists of sandy beaches and coastal wetlands, particularly in
4 the area of the Delta Po Plain. The coasts are affected by a marked natural subsidence, because of
5 tectonic processes and recent sediments consolidation. Since the second half of the last century, the
6 subsidence in coastal area has increased significantly due to intense human activity, namely gas
7 extraction and groundwater exploitation.

8 The work presented in this paper aimed at investigating the temporal evolution of patterns and
9 processes on a stretch of coast located between Lido di Dante and Lido di Classe, including the
10 mouth of the Bevano river near Ravenna (Italy), using remotely sensed datasets. An innovative
11 integration of remote sensing and monitoring method (Permanent Scatter Interferometric Synthetic
12 Aperture Radar - PSInSAR, Small BAeline Subset - SBAS and Empirical Orthogonal Function –
13 EOF analysis of 20 years of Landsat) has been used to study the temporal evolution of subsidence
14 and its correlation with natural and anthropogenic causes. Results show an increase of the
15 subsidence rates obtained for the last decade: the amount of subsidence due only to natural causes is
16 typically a few millimeters per year, while the man-induced subsidence reaches values of several
17 millimeters per years. Marshlands reclamation, groundwater pumping for agricultural and industrial
18 purposes and methane extraction from gas fields near the coastline are the principal anthropogenic
19 causes. Subsidence in combination with sea level rise will get worse inundation risk from the rivers
20 and widens the coastal areas affected by storm surges and tidal inundation. This makes subsidence
21 an insidious threat having significant cumulative effects on flood risk or the integrity of water
22 defenses and infrastructure.

23

24 *Keywords: Subsidence, Coastal Areas, Remote Sensing, Permanent Scatter, Monitoring, Underground*
25 *water, Vegetation.*

26

27 **1 INTRODUCTION**

28 Subsidence in coastal areas and its relation to sea-level rise is a relevant geological, ecological and
29 geomorphological process that also has implications for coastal ecosystems because it may generate
30 increased sea-water flooding and salinisation of coastal aquifers and an instability of levees and
31 infrastructure (Hallegate et al., 2013). Subsidence is a downward displacement of the land relative
32 to sea level, and it often occurs in regions associated with alluvial sediments, such as a deltaic area
33 or alluvial plain; these regions typically have thick Quaternary deposits comprised of clay and
34 sandy loam (Chen and Rybczyk, 2005).

35 The holistic view of the environment that scientists apply when studying and interpreting landscape
36 evolution is based on the principle that the scale of observations of certain physical processes
37 determines the level at which spatial patterns of landscapes can be explained. This means that a
38 physical process, such as subsidence may influence ecosystem functioning generating disturbance
39 and determine perturbations or stress within the coastal vegetation growth (Temmerman et al.,
40 2003). Disturbance and perturbation (D'Alpaos et al., 2012; Nicholls et al., 2011) are widely used
41 to describe the evolution of a natural system (receptor), and they allow the role of other parameters
42 to be considered, such as subsidence in the final landscape analysis (Marquenie and de Vlas, 2005;
43 Syvitski et al., 2009; Taramelli et al., 2013, 2014a).

44 The action of natural hazards is the 'cause' of disturbance when they drive disruption and losses,
45 and their action is simultaneously the 'effect' of disturbance when it produces changes in the main
46 pattern of vegetation after extreme events (Evans et al. 2004; Passalacqua et al., 2013; Van
47 Wesenbeeck et al., 2008;). Subsidence in this context can be considered a complex source of
48 alterations in the steady states of a system; therefore, a reference state of a subsiding ecosystem
49 must be defined spatially and temporally (Taramelli et al., 2013a). Although the spatial influence of
50 subsidence can be wider than the specific area of interest because of subsequent flooding and
51 erosion, it can be defined with different levels of precision based on the spatial scale of observation.
52 When referring to ecosystem functions such as vegetation gain and loss, the temporal scale becomes
53 increasingly important because the steady state of a subsiding vegetated ecosystem must be fixed
54 (D'Alpaos et al., 2012; Marani et al., 2006; Taramelli et al., 2014b; Temmerman et al., 2007).
55 Temporal observations include defining the disturbance typology that can be considered as chronic
56 or continuous and specific conditions of disturbance that generate perturbation or stress. A
57 continuous rate of subsidence determined at large temporal scales shows adapted vegetation with
58 species that are resistant to altitude variation; however, at a shorter temporal ranges such as groups
59 of rainless years, the intervention of higher rates of subsidence can drive the extinction of some of
60 the most sensitive species (Taramelli et al., 2011; Van Dobben and Slim, 2005; 2012).

61 Moreover, subsidence in dynamic ecosystems such as coasts can sometimes represent the
62 continuous inputs required to maintain the viability and organisation of living components. This
63 means that there are ecosystems in a non-equilibrium state that are responding continuously to
64 environmental gradients (rainfall, subsidence) and ecological interactions (competition and
65 extinction – Taramelli et al., 2014b). Normal forcing and processes become disturbances when the
66 nominal bounds are exceeded (Corenblit et al., 2011; Pimm, 1984). Therefore, the challenge is not
67 only in determining how subsidence is a cause and effect disturbance but also in establishing when
68 a normal forcing becomes a disturbance by establishing thresholds. Another aspect in analysing the

69 feedback between subsidence and coastal vegetation is that disturbances are not strictly negative
70 phenomena; when disruptive events free resources or open corridors for species cross-changes, the
71 biodiversity and stability of communities can increase (Reinhardt et al., 2010). Stress is an effect of
72 disturbance and can be considered a specific perturbation characterised by specific variations from
73 the steady state induced by the propagation of disturbance (Antonellini and Mollema, 2010;
74 D'Alpaos et al., 2012; Marani et al., 2010; Wang and Temmerman, 2013). These phenomena occur
75 both for natural and anthropogenic reasons that may have a synergic effect and increase the total
76 displacement for heavily populated coastal lowland areas in particular. Natural subsidence that
77 results from autocompaction of sediment under its own weight is enhanced by sub-surface fluid
78 withdrawal, drainage and ground overburden that increase the potential for inundation, coastal
79 erosion, habitat disruption and salt-water intrusion. As summarised by Chen and Rybczyk (2005),
80 coastal subsidence in these depositional zones is a function of five processes: (1) downwarping, (2)
81 tectonic activity, (3) consolidation of Tertiary, Pleistocene, and Holocene deposits, (4) shallow
82 subsidence, and (5) underground water and gas extraction (Taramelli et al., 2014a). When only
83 natural processes are considered, the combination of 1, 2, and 3 defines deep subsidence, and
84 shallow and deep subsidence combined equal the total subsidence (Cahoon et al., 1995; Tosi et al.,
85 2012).

86 Improvements by new monitoring techniques that produce more accurate results by remote sensing
87 have increased the study of the spatial and temporal evolution of this phenomena and allowed the
88 construction of a series of simulation models designed to reduce risks to the environment. As stated
89 by Hung et al. (2010), considerations when selecting a monitoring system are a 1) high spatial
90 sampling density, 2) good measurement accuracy and 3) high temporal frequency. However, the
91 selection is usually made according to the available funding. Various methods have been used for
92 measuring and mapping the spatial gradients and temporal rates of regional and local subsidence
93 and horizontal ground motion (Galloway et al. 1999; Tosi et al., 2013). The methods generally
94 measure relative changes in the position of the land surface, and the observable position is typically
95 a geodetic reference mark that was established so that any movement can be attributed to deep-
96 seated ground movement rather than surficial effects.

97 Interferometric synthetic aperture radar (InSAR) analysis (Bamler and Hartl, 1998; Rosen et al.,
98 2000) is a remote sensing technique that takes into account a multi-temporal systematic acquisitions
99 and wide spatial coverage; these features make them particularly useful for regional monitoring,
100 such as what is required for the analysis of coastal areas. Therefore, this technique has been
101 discussed in a large number of publications, and practical applications have been developed for
102 coastal environments. In particular, urban and peri-urban coastal areas have been extensively

103 studied with this technique, with case studies such the Venice Lagoon, the Nile River Delta,
104 Taiwan, New Orleans (Bock et al., 2012; Hung et al., 2010) and Indonesia, where the subsidence
105 rate was clearly related to groundwater and gas extraction using the InSAR method (Chaussard et
106 al., 2013). InSAR exploits SAR data, which can be divided into 2 main categories: 1. large coverage
107 area (100 km) and long revisiting time (35 days); 2. small coverage area (40 km) and short
108 revisiting time (4-11 days). ERS and Envisat belong to the first category, whereas Cosmo Sky Med
109 and TerraSar-X belong to the second.

110 In coastal areas, SAR-based techniques, such as interferometric SAR (interferometric synthetic
111 aperture radar (InSAR)), persistent scatterer interferometry (PSI), permanent scatterer (Ferreti et al,
112 2001), SBAS (Berardino et al 2002), and interferometric point target analysis (IPTA) (Strozzi et al
113 2003), are integrated into a Subsidence Integrated Monitoring System (SIMS) to overcome the
114 limits characterising each technique. The Venice Lagoon is an area where SIMS efficiently merged
115 the different displacement measurements obtained by high precision-levelling, differential and
116 continuous global positioning system (GPS) data, and synthetic aperture radar (SAR)-based
117 interferometry to obtain information on land deformation from 1992 to the present (Tosi et al.,
118 2009; Chaussard et al., 2013).

119 In this paper, the use of data from the “Extraordinary Plan of Environmental Remote Sensing” by
120 the Italian Ministry of Environment (Ministero dell'Ambiente e della Tutela del Territorio e del
121 Mare - MATTM) shows that the PSInSAR technique integrated with a SBAS temporal analysis and
122 can produce extremely accurate (mm per year) results in vertical resolution that are consistent with
123 the results obtained by other absolute measurement techniques, such as GPS and topographic
124 levelling.

125

126 **2 DESCRIPTION OF THE STUDY AREA**

127 **2.1 Geologic, geomorphologic and hydrogeological settings**

128 The Foce Bevano is a small fluvial outlet located in the northern Adriatic near the town of Ravenna
129 (Figure 1). The Bevano is a river with a catchment area of 92.5 km² (Balouin et al., 2006) and total
130 length of 34 km. The site is located in a densely populated area (south of the Po Delta) that is also
131 one of the most important natural environments along the northern Adriatic coast where natural
132 geomorphological dynamics control a non-urbanised stretch of approximately 5 km. The river
133 mouth is characterised by ecologically important habitats, such as wetlands, pinewoods, sandy
134 beaches and sand dunes. This relatively minor watercourse forms a small-scale estuarine system
135 because the tidal excursion is limited along the Italian coasts, so large-scale estuaries are almost
136 absent.

137 Over the past 50 years, the Bevano area has undergone major morphological changes (Armaroli et
138 al., 2013), which has allowed the study of its evolution and dynamics. In particular, its mouth
139 underwent a rapid northward migration as a result of the dominance of marine processes, such as
140 alongshore currents, coupled with a low energy fluvial regime. During these years the river mouth
141 has been losing hydraulic efficiency, also because the river has become completely controlled and
142 flooding avoided. This has led to the prevalence of marine processes at the mouth, with the outlet
143 behaving essentially as a tidal inlet, seasonally closed especially after storms (Baloian et al., 2006,
144 Sedrati et al., 2011). Moreover, the channel migration caused a rapid erosion of the dunes located
145 immediately north of the mouth. Therefore, an intervention of artificial stabilisation was necessary
146 along the stretch of coastline. In 2006, the mouth of the river was closed and re-opened 500 m south
147 (Gardelli et al., 2007), while the dredged sand was used to reconstruct dunes. Since then the system
148 has been reasonably stable, also because the northern bank is partially protected by environmentally
149 friendly timber training structures. Only minor works of repairs were done in the last few years
150 (Ciavola et al. 2012).

151

152

153 *Figure 1 - Landsat satellite image (16/07/2003) of the Northern Adriatic coast (on the left) and the study site*
154 *Foce Bevano (on the right).*

155

156 In the stratigraphic classification, the deposit outcropping of the post-evaporite succession are part
157 of the Supersynthem Emiliano-Romagnolo, which is the stratigraphic unit that includes the late-
158 Quaternary sediments of the Po Plain (Ricci Lucchi et al., 1982). This Supersynthem includes the
159 Sintema Emiliano-Romagnolo Inferiore (AEI) and the Sintema Emiliano-Romagnolo Superiore
160 (AES) (Cibin et al., 2005). The AEI is the oldest part of Supersynthem; however, it is not present in
161 any of the outcrops. In contrast, the AES represents the upper portion of the Supersynthem, and all
162 of the continental sediment outcroppings can be identified. Climatic and eustatic fluctuations have
163 conditioned the sedimentary dynamics in Northern Adriatic (Correggiari et al., 2005). In effect, the
164 subsoil contains the cyclic alternation of organic clays, silts, sands and gravels. The AES is divided
165 into additional subsynthem that correspond to recent deposits that are related to the transgressive
166 and regressive sea phases that occurred during the Quaternary (Cibin et al, 2005). The Modena Unit
167 (AES8a) emerges in the mouth of the Bevano River and represents the top part of the Ravenna
168 Subsynthem (AES8). The AES8a is composed of surficial and more recent sediments, including
169 those currently in progress, which are several meters thick (maximum 10 m).

170 The Ravenna Subsynthem consists of fluvial gravels covered by clay, silt and sand that have a
171 tabular geometry and average thickness of 25-30 m. The top of the Ravenna Subsynthem coincides

172 with the topographical plan, and the basal portion is characterised by the presence of sediments rich
173 in organic matter (Cibin et al, 2005). The origin of these sediments dates to the late Pleistocene in
174 the post-Wurmian glaciation. From the documentation of its subsurface geology, which is available
175 in the geognostic database and the work of Aquater (1988) and Iter (1989), the Ravenna
176 stratigraphy is composed of alternating layers of sand, silt and organic matter.

177 The stratigraphy can be summarised as follows:

- 178 • up to 10 m, there is an alternation of sandy layers with thin layers of silt and peats;
- 179 • from -10 to -25 m, the clayey silts become sandy silt with increasing depth; and
- 180 • from -25 to -30 m depth, there are silt clays and clayey silts with rare coarse sandy lenses.

181 According to Regione Emilia-Romagna & ENI-AGIP (1998), the Sintema Emiliano-Romagnolo
182 Superiore (AES) hosts 4 main aquifer complexes: A1, A2, A3, and A4. Above these aquifers is a
183 shallow unconfined aquifer (A0). In detail, the hydrogeology of the coastland is characterised by a
184 multi-layered aquifer system confined between aquitards. The sediments related to the transgressive
185 and regressive sea phases constitute the aquifers and aquitards. The aquifers are composed
186 primarily of sandy lithotypes, whereas the aquitards are composed of silty-clay sediments. Figure 2
187 shows the distribution of deep aquifers in the Foce Bevano area as proposed by Regione Emilia-
188 Romagna & ENI-AGIP (1998). Data from the groundwater monitoring network of ARPA Emilia-
189 Romagna show that the deep coastal aquifers of the Ravenna coastland before the 1980s were
190 heavily used for industrial and agricultural pumping. The pumping of an aquifer produces both
191 elastic and inelastic land compaction (Meinzer, 1928; Jacob, 1940; Cernica, 1995; Domenico and
192 Schwartz, 1998; Sun et al. 1999). In a hydrogeological system comprised of aquifers separated by
193 aquitards (silty-clay sediments), such as in the Ravenna coastland (Fig. 2), the lowering of pore-
194 water pressure induced by groundwater withdrawals allows the fine-grained particles to compress
195 or compact (Poland, 1984). The compaction process of aquitards may continue long after the
196 stabilisation of drawdowns (Galloway et al., 1999). If the pore-water pressure recovers (e.g.,
197 withdrawals are stopped), the elastic compaction can be gradually recovered; however, the inelastic
198 compaction becomes permanent (Sun et al., 1999; Galloway et al., 1999). Data from the pumping
199 well (RA36-00, 500 m from the dunes; see Fig. 2 for the localisation) show that since the early
200 1980s, the reduction of pumping allowed the deep aquifer to recover approximately 16 m; by the
201 late 1990s, the depth was -6 m. The piezometric data refer to the A3 deep confined aquifer (Fig. 2)
202 (Regione Emilia-Romagna & ENI-AGIP, 1998). Based on this evidence and considering all of the
203 piezometric data available in the Ravenna coastland, a general rise of the potentiometric surface
204 was observed after the 1980s (Fig. 4c). The piezometric data are consistent with the rising of
205 groundwater levels in the Ravenna coastland discovered by Teatini et al. (2005) in which the

206 potentiometric surface induced by the well closures that occurred after 1980s produced a pore
207 pressure recovery in the coastal multi-aquifer system. After the well closures, the rates returned to
208 similar levels as registered before World War II (Carbognin and Tosi, 2003; Teatini et al., 2005).

209

210

211

212 *Figure 2 – Main aquifers in the Foce Bevano area with the location and characteristics of wells monitored*
213 *by ARPA Emilia-Romagna. The hydrostratigraphic section is modified from Regione Emilia-Romagna &*
214 *ENI-AGIP (1998). The meaning of the symbols are as follows: 1) aquifers hosted by the Sintema Emiliano-*
215 *Romagnolo Superiore (A1, A2, A3, and A4); 2) highest aquifer of the Sintema Emiliano-Romagnolo Inferiore*
216 *(B1); 3) aquitards; 4) salty waters; 5) Tyrrhenian transgression; 6) boundary of aquifer complexes; 7) salt-*
217 *freshwater interface; 8) gas wells; and 9) water wells (piezometers).*

218

219

220 **3 DATA SOURCES AND METHODOLOGY**

221 The basic methodology uses an RS time-series to analyse the (a) subsidence trends in coastal
222 evolution over time and (b) time series of spatial patterns in coastal vegetation for improved
223 ecosystem analyses. Specifically, the methodology considers examples of properties that are the
224 best proxy for characteristics of emerged and shallow submerged coastal areas by combining multi-
225 sensor space-borne remote sensing (SAR and optical).

226 A data set of Landsat TM and ETM+ imagery (from U.S. Geological Survey) was acquired to
227 analyse the main spatial and temporal patterns of change that characterise the study site. Based on
228 archive availability (Table 2), the covered time span ranged from 1991 to 2011 for Bevano (Figure
229 4). The radiometric calibration and conversion from digital numbers to exoatmospheric reflectance
230 were performed according to Chander and Markham (2003) and Chander et al., 2009 to normalise
231 for variations in illumination conditions and solar irradiance and compensate for seasonal variations
232 in Earth-Sun distance.

233 As a result of the widespread subsidence phenomena affecting the area (Taramelli et al., 2013a), an
234 additional time-series of SAR (synthetic aperture radar) data (ERS-1/2 satellites – Table 3) was
235 collected from Foce Bevano from 1993 to 2000 (Table 4), and we produced deformation maps of
236 coastal morphology through the small baseline subset (SBAS) algorithm (Berardino et al., 2002).
237 To validate these results and quantify the evolution of the subsidence trend in the following
238 temporal interval (2003-2010), we also used additional interferometric data contained in the
239 “Extraordinary Plan of Environmental Remote Sensing” by the Italian Ministry of Environment
240 (Ministero dell'Ambiente e della Tutela del Territorio e del Mare - MATTM). The database consists

241 of deformation measurement points obtained from a time series of 90 ERS1-ERS2 and ENVISAT
242 images (acquired from 1992-2000 and 2003-2010, respectively) and calculated using the PSInSAR
243 (Permanent Scatterers) technique (Ferretti et al., 2001).

244 The interferometric data consist of a database of deformation measurement points obtained from the
245 processing of satellite images (ERS1-ERS2 and ENVISAT) acquired from 1992-2000 and 2003-
246 2010, respectively. The overlap of the PS distribution on the geographical bases produces a first
247 interpretation phase, which is the identification of zones in motion (unstable areas). All of the
248 deformation measurements are classified according to their displacement velocities measured along
249 the line of sight (LOS), and they are relative because the deformation is calculated with respect of a
250 reference point position; therefore, the measurements are considered stable and validated by
251 comparing with the available GPS measurements. The measured displacement represents the
252 difference between the PS position during the reading and the acquired reference. The processing
253 allows for the determination of the deformation velocity of each target, which assumes a linear
254 model of deformation in the time. In the mouth of the Bevano, the permanent scatterers correspond
255 to existing structures that are man-made (roads, buildings, roofs, and metal structures) or natural
256 points that are stable in time (rock outcrops, debris and slopes).

257

258 **3.1 Trends in coastal evolution over time: DInSAR Analysis for Subsidence detection**

259 *SBAS-DInSAR data analysis and measurement of active ground deformation in the Bevano area*

260 To investigate the present deformation rates at the Bevano study site, we adopted the multi-
261 temporal differential interferometric SAR (synthetic aperture radar) technique. The classical
262 technique differential SAR interferometry utilises SAR image data to calculate the ground surface
263 movements that eventually occur between two different passes of a satellite over the same area, and
264 it is based on the radar concept, which is the phase of the radar signal that is returned as the satellite
265 conveys quantitative information on changes in the sensor-to-ground distance (range) caused by
266 deformations of the surface (Bürgmann et al., 2000). By subtracting the phase of the two images
267 and then simulating and subtracting the phase contribution that results from the topographic relief (a
268 DEM is required), a differential interferogram is formed that contains the ground deformation
269 signal that occurred in the interval between the two passes (Massonnet and Feigl, 1998). The
270 DInSAR technique measures the phase changes between two separate acquisitions of the same area
271 in similar geometric conditions. With this technique, it is possible to identify any differences as a
272 result of deformation phenomena, topography or atmospheric disturbances (Massonnet and Feigl,
273 1998). The objective is to isolate the phase contributions that result from actual surface movements
274 from the contributions caused by disturbance. The phase difference in the electromagnetic wave is

275 key to identifying the areas subject to surface movements. The accuracy of surface movements
276 measured by the DInSAR technique depends on various factors (atmospheric effects, orbital effects,
277 stability of ground scatterers, unwrapping errors, etc.); however, in favourable cases, the accuracy
278 of the displacement measures can be up to a centimetre (Hanssen, 2001). The SBAS technique
279 needs a high number of coregistered SAR data to work with differential interferogram series, which
280 are characterised by a small spatial distance between orbital positions (spatial baseline). This
281 geometric constraint limits the spatial decorrelation and topographic errors (Zebker and Villasenor,
282 1992). Through a series of differential interferograms, it is possible to obtain a velocity map of
283 deformation and displacement time series. This technique allows quantifying average displacement
284 per annum per each coherent pixel with accuracy on the order of millimetres (Berardino et al. 2002;
285 Lanari et al. 2004).

286 In this work, we used the small baseline subset (Berardino et al. (2002) algorithm. By using SBAS,
287 we exploited the large amount of SAR data acquired by the ERS-1/2 satellites of the European
288 Space Agency (ESA) since 1992 to estimate the displacement time-series and mean velocities of
289 coherent areas of the ground (Tolomei et al., 2013). The SBAS concept utilises a large number
290 (several tens) of radar images to reduce the various noise components of DInSAR interferograms
291 and increase the accuracy of the displacement measurements. Initially the operator defines the
292 acceptable temporal and orbital separations occurring between the images of each DInSAR
293 interferogram to be generated. Then, a consistent number of differential interferograms are
294 generated using a DEM of comparable resolution and unwrapped to generate the actual
295 displacement maps. Then, the reference pixel that will be used by all of the calculated
296 displacements and velocities is selected, and the singular value decomposition (SVD) technique is
297 used to invert the unwrapped phases to retrieve the displacement time series at each image date for
298 each pixel showing a coherence value larger than a fixed threshold. The SVD algorithm is used to
299 compute the matrix pseudoinverse to solve the over-determined linear equation system. During this
300 step, the orbital residual and topographic errors are estimated and then subtracted. Finally, double
301 filtering in time and space is conducted and the short-term atmospheric contribution is removed. In
302 our SAR data processing, only the pixels showing an interferometric coherence larger than 0.7 over
303 a minimum of 35% of the total number of the interferograms were considered reliable (Bürgmann et
304 al., 2000). In fact the coherence value is a quality marker for each pixel because states how much a
305 target keeps stable its physical characteristics and therefore its response to the radar impulse. So, for
306 each retained pixel with 80 x 80 m dimensions on the ground, a time series of the ground
307 displacements was calculated. All of the displacements were relative to the reference pixel (or area),
308 which was assumed to be stable in the image (Bürgmann et al., 2000) and along the sensor line of

309 sight (LoS). It is important to highlight that for each pixel on the surface we obtain displacement
310 measurements along the satellite Line of Sight with very high accuracy (resolution) up to 1-2 mm.
311 The retrieved displacement represents the difference of the distance between the target and the
312 sensor position at the two acquisition times (Burgmann et al., 2000; Massonnet and Feigl, 1998).
313 We applied the SBAS technique to a data set of 36 ERS-1/2 images acquired on the descending
314 pass in the period from 10/5/1992 to 29/12/1999 (Track 122, Frame 2704). We applied a
315 multilooking process because radar images are affected by a form of noise that degrades the quality
316 of the image itself (speckle). Averaging over the range and/or azimuth resolution cells may generate
317 multilook images. The subsequent improvement in radiometric resolution from the multilooks
318 causes an associated degradation in spatial resolution. In our case, we adopted a number of looks
319 equal to 20 in the azimuth direction and 4 in the range direction. Finally, for the generation of the
320 DInSAR couples, we imposed a maximum orbital separation of 300 meters to reduce the spatial
321 decorrelation and a maximum temporal distance between two passes of 1000 days to limit the
322 effects of temporal decorrelation; using these constraints, 85 interferograms were generated. We
323 used the SRTM DEM for the topography subtraction (<http://www2.jpl.nasa.gov/srtm> - Farr et al.
324 (2007)) with a ground posting of 80 x 80 m per pixel.

325 326 ***PSInSAR data set of active ground deformation in the Bevano area***

327 The displacement time series, which were provided by the Italian Ministry of Environment through
328 the Extraordinary Plan of Environmental Remote Sensing, were calculated using the PSInSAR
329 (permanent scatterers) technique (Ferretti et al., 2001). This technique was based on observations of
330 the phase-stable pointwise targets called permanent scatterers (PS), which were detected through a
331 statistical analysis of the amplitudes of their electromagnetic returns. The PS outputs included the
332 average displacement rates over the observed period and time series of the deformation per each
333 point with a high coherence of the area, and they provided information on the temporal evolution of
334 the displacements. The average displacement rates were measured along the sensor's line of sight
335 (LoS) and calculated with respect to the position of a ground reference point, which was considered
336 to be stable over time and with coordinates known through GPS measurements. The measured
337 displacement was the difference between the PS position in each image with respect to the reference
338 acquisition. The processing allowed for the determination of the deformation velocity of each
339 target, assuming a linear model of deformation in time.
340 The space-time characterisation of ground deformations was achieved through the displacement
341 time series. This analysis evaluated the deformation trend of individual PS and extended beyond the
342 information obtainable from the velocity values alone (MATTM, 2009). For the period 1992–2010,

343 the displacement time series was derived through a standard analysis that involved the use of a
344 linear model to describe the target movements (T.R.E., 2008). The time series showed the
345 displacements measured in mm along the LoS for a given PS as a function of the time elapsed since
346 the first reference acquisition.

347

348 **3.2 Time series of spatial patterns in coastal vegetation**

349 *Spectral mixing analysis (SMA)*

350 Among the processing techniques, one of the most suitable in heterogeneous environments is
351 spectral mixing analysis (SMA) because of its quantitative results on the fractional abundance of
352 pure components within each pixel. It represents the spatial variation below the sensor resolution
353 without assigning each pixel to a single class, such as in “hard” classifications (Taramelli et al.,
354 2013b).

355 SMA is a technique that can consider sub-pixel variation in surface components. The methodology
356 is based on the observation that radiances from surfaces with different ‘endmember’ reflectances
357 usually mix linearly in their proportion to the area of the field of view. Therefore, if a limited
358 number of distinct spectral endmembers can be found, it is possible to define a mixing space where
359 mixed pixels can be described as linear mixtures of these endmembers. SMA allows for the
360 estimation of the endmember fractions that best fit the observed mixed reflectances (Boardman,
361 1989; Small, 2004).

362

363 *Change detection analysis from NDVI and SMA*

364 We applied a univariate image differencing technique (Coppin et al., 2004; Lu et al., 2004; Singh,
365 1989) to assess the type, strength and spatial pattern of changes as described by each remotely
366 sensed imagery. From each Landsat image, we derived the normalised difference vegetation index –
367 NDVI (Goward et al., 1991), which was calculated as the ratio between red and near-infrared
368 radiance [$NDVI = (NIR - RED)/(NIR + RED)$ where NIR (i.e., Landsat band 4) and RED (i.e.,
369 Landsat band 3) are the amounts of the near-infrared and red light, respectively, that are reflected
370 by the vegetation and captured by the sensor of the satellite]. NDVI is recognised as an important
371 index of ecological relevance (Kerr and Ostrovsky, 2003), and its relationships with vegetation
372 productivity, which is the fraction of absorbed photosynthetic active radiation intercepted (fAPAR),
373 biomass and phenological patterns are well documented (Pettorelli et al., 2005). For each interval, a
374 new image was obtained based on a standardised difference (Zurlini et al., 2006a; Zurlini et al.,
375 2006b) between $NDVI_{t1}$ and $NDVI_{t2}$, which are the NDVI images at time t_1 and t_2 .

376 The NDVI change over time is a continuous variable; to obtain a binary (i.e., change, no change)
377 map, a threshold of change must be defined; in this study, it was set to a percentile of 10% (5% on
378 each tail) of the empirical standardised difference distribution according to Zurlini et al. (2006a,
379 2006b). Whenever a pixel value in $\Delta\text{NDV}_{t1,t2}$ was less than the 5% percentile of positive values, it
380 was marked as a change.

381 In addition to a change detection analysis using NDVI, a fraction of the vegetation from SMA has
382 been used to obtain a concurrent change detection analysis. The aim was to obtain a more sensitive
383 detection of changes to solve the signal of mixed pixels, which consist of several reflectance
384 elements that depend on the physical composition of the investigated surface and not just the
385 absorbed photosynthetically active radiation intercepted by plants. This approach provides a
386 powerful tool for deciphering the information contained inside each pixel, and it can isolate changes
387 in natural (e.g., halophytic) vegetation from changes in classes (e.g., agricultural lands).

388

389 *Trend analysis (EOFs)*

390 To characterise the temporal trends in vegetation, a time series of vegetation fractions (obtained
391 from the spectral mixing analysis) was analysed to discriminate the interannual signal of vegetation
392 changes in both space and time. To this end, empirical orthogonal functions (EOFs) (Lorenz, 1956;
393 Bjornsson and Venegas, 1997; Hannachi et al., 2007; Taramelli et al., 2013a; 2013b) have been
394 applied. In signal processing, this method includes the decomposition of a signal or data set in terms
395 of orthogonal functions, which allow us to determine the spatial patterns of change and their
396 variation and evolution over time. In addition, it can provide a quantitative measure of the
397 contribution of each of these patterns to the overall multi-temporal change. The aim is to isolate the
398 different components contributing to change within the time series and assign a value of relative
399 importance to each one of them.

400 Change detection measures the variation in vegetation cover between two instances by subtracting
401 two discrete values, and the EOF analysis can quantify spatial variability patterns and their temporal
402 evolution year by year while also providing a measure of the importance of each pattern with
403 respect to the whole time-series. The EOF analysis of the vegetation fraction maps allowed us to
404 investigate the main trends of evolution in the decades of interest.

405 To perform this analysis, we produced a spatio-temporal matrix in which each row corresponded to
406 one year (image acquisition) in the time series and each column was a time series of each pixel
407 (fraction value). In each row, we listed the vegetation fraction values associated with all of the
408 pixels of each image in the analysed time span. The second step was to calculate a new matrix by
409 multiplying the matrix by its transposed matrix. The new matrix was detrended (its mean was

410 subtracted), and the eigenvectors and eigenvalues were then calculated. The eigenvectors
411 corresponded to the empirical orthogonal functions, and the eigenvalues represent the variance
412 associated with each eigenvector and give a measure of the importance of each EOF to the total
413 changes over the entire period of time. The outputs are a dimensionless map of change in the study
414 area, and the expansion coefficients represent the evolution of the phenomena during the time
415 period. The time evolution of an empirical orthogonal function shows how the pattern obtained in
416 the analysis oscillates in time. The evolutions of EOFs in time are referred to as expansion
417 coefficients, which are uncorrelated in time. The analysis of the expansion coefficients led to the
418 identification of peaks, both positive and negative, in the vegetation evolution over the time series.
419 We thus applied a change detection to these smaller time frames, or particular years of interest, to
420 quantify the vegetation changes.

421

422 **4 RESULTS**

423 **4.1 Subsidence using PSInSAR and SBAS**

424 The retrieved ascending mean velocity map from SBAS is shown in Figure 3a in which the image
425 pixels are symbolised as points. Because of the low relief, diffuse vegetation cover and scarcity of
426 rock outcrops, the level of temporal coherence is rather low in the area, and only a few pixels reach
427 the minimum coherence level of 0.7. During the processing, all of the displacement time series are
428 calculated with respect to the position of a ground reference point, which is considered to be stable
429 over time and with coordinates known through GPS measurements. We selected such a reference
430 area near flat areas where no geomorphological evidence of long-term subsidence could be found
431 (Teatini et al., 2005; Taramelli et al., 2013a). The surface movements measured using DInSAR
432 techniques are always scalar measurements along the line of sight of the satellite (Bürgmann et al.,
433 2000). In our case (ERS imagery), the LoS is inclined approximately 23° from the vertical and
434 looks to the east from the ascending orbit, i.e., a line running N13°W.

435 Our results (Figure 3a) indicate that from 1992 to 2000, the ground in the central and upper part of
436 the Bevano moved away from the satellite with rates of up to 5-8 mm/year, whereas the nearby
437 areas located outside of the Bevano limits were relatively stable. From the field observations and
438 geological setting, the main horizontal component of the movement was perpendicular to the main
439 flat direction, whereas a negligible deformation occurred along the direction of the slope. Such
440 movements that occur almost parallel to the ascending orbit cannot be resolved in DInSAR
441 interferograms because they only cause a small change of distance between the SAR antenna and
442 ground (Bürgmann et al., 2000). Therefore, we can safely assume that the displacements resulting
443 from our SBAS analysis represented the projection in the LoS of the vertical component of ground

444 deformation, and we can calculate the actual vertical displacement or velocity by simply dividing
445 the LoS value by 0.9 (cosine of the local incidence angle).

446

447

448 *Figure 3 - (a) Ground velocity map (mm/year) of deformation calculated between 1993 and 2000 using the*
449 *SBAS methodology, (b) between 1992 and 2000 using PSInSAR on ERS1-ERS2 data, and (c) between 2003*
450 *and 2010 using PSInSAR on ENVISAT data.*

451

452 In Figure 3b and 3c, we show the average displacement velocities for the permanent scatterers in
453 the Po Delta and adjoining coast from the ERS-1/2 and ENVISAT dataset. The results show that in
454 both maps, the PS located along the coast and near the river outlets have higher displacement rates
455 compared to inland areas, which are relatively stable. In the 1992-2000 period, the PSInSAR
456 velocities are consistent with our SBAS results, and the measured rates are comparable in both
457 methodologies. Both results support the findings that the Bevano area moved away from the
458 satellite, whereas nearby areas were relatively stable. In addition, the PSInSAR results for 2003-
459 2010 show an increase in the rate of negative displacement when compared with the period 1992-
460 2000. In fact, in the 2003-2010 ENVISAT dataset, a large number of unstable PS are found to move
461 away, with rates between -19.5 and -6.6 mm/year. A detailed analysis on the Bevano outlet between
462 2003 and 2010 confirms the trend towards negative velocities (Figure 4b). The resulting total
463 displacement trend, considering both PS, indicates a lower of the ground of approximately 80 mm
464 occurred from 1992-2010. The retrieved displacement represents the difference of the distance
465 between the target and the sensor position at the two acquisition times (Burgmann et al., 2000;
466 Massonnet and Feigl, 1998). It is important to highlight that for each pixel on the surface (spatial
467 resolution) we obtain displacement measurements along the satellite Line of Sight with very high
468 accuracy (resolution) up to 1-2 mm in the retrieved vertical displacement. Further details on the
469 causes that produced the increase of ground subsidence in the last decade are discussed in the
470 Discussion section.

471

472 *Figure 4 — Map of average displacement rates of the (a) ERS-1/2 and (b) ENVISAT PS, which were located*
473 *around Foce Bevano. In the period 2003–2010, a greater number of PS is observed as moving away from the*
474 *sensor with rates higher than before 1992–2000, which likely indicates an increase in terms of subsidence.*
475 *(c) Piezometric level of well RA36-00 (red triangles, see Fig. 2 for localisation) and displacement time series*
476 *(black circles) in Foce Bevano from 1992 to 2010.*

477

478

479

480 **4.2 Change detection from NDVI and SMA**

481 The NDVI change detection in Foce Bevano from 1991 to 2011 led to a map with no extensive
482 areas of change and sparse vegetation patches where gains and losses in biomass occurred (Figure
483 5). Near the mouth and along the meandering course of the river, relatively unstable riparian and
484 halophile vegetation areas can be detected. For both the riparian and pine forest vegetation classes,
485 the majority of pixels shows no change (81.56% and 91.86%, respectively), whereas vegetation
486 increased by 7% and 1%, respectively.

487

488

489 *Figure 5 – Change detection in the decades 1991-2011 based on NDVI.*

490 Change detection using SMA led to the identification of a higher number of gain and loss pixels,
491 where they were classified as “no change” pixels using only the NDVI (Figure).

492

493 *Figure 6 – Change detection in the decades 1991-2011 based on vegetation fraction from SMA.*

494 Therefore, the Bevano area appears more strongly changed in terms of halophilic and riparian
495 vegetation. The loss and gain values are consistent with the results obtained from the NDVI-based
496 analysis and correspond to the high degree of change that occurred in the mouth region during the
497 last two decades. To calibrate the particular value of gain and loss of vegetated areas that
498 corresponds to the subsidence areas, we examined the distribution of values at numerous locations
499 where a high subsidence rate in the period 1993-2000 was found. This multi-temporal analysis
500 showed higher displacement rates in which wetland hydrology is more strongly influenced by
501 anthropic activities.

502 At these sites, 9% of the loss in total vegetation value served as an accurate threshold for
503 delineating the signature of the vegetation loss within the subsidence pixels.

504 The spatial component of the first EOF in Foce Bevano shows that the areas affected by major
505 changes in vegetation distribution are those located along the coast and near the river outlet (7a).

506 The graph of the temporal component, which represents 77% of the dataset variance, shows that the
507 trend is affected by strong fluctuations in the initial period of analysis between 1991 and 1994 and
508 between 1996 and 1998. The peak in 1998 may be correlated to the beginning of the accelerated
509 subsidence rates in the area, which is shown in the InSar time series analysis.

510

511

512 *Figure 7 – Temporal and spatial component of the three EOF in Foce Bevano.*

513 The second EOF in Foce Bevano, which explains approximately 3% of the total variance, shows the
514 greatest variation patterns around the mouth of the river (Figure 7b). Its temporal component shows
515 a more cyclical trend that becomes greater in amplitude between 2003 and 2006 when the most
516 rapid migration of the mouth occurred, which led to the destruction of more than 150 m of dunes
517 and part of the pinewood (Armaroli et al., 2013). To notice also the occurrence of an exceptional
518 storm in September 2004, which, as documented by Ciavola et al. (2007) caused widespread
519 erosion of the beach-dune system in the area north of the Bevano. The capacity of recover of
520 vegetated communities is evident by the inverted trends observed after the 2006 intervention. As
521 already detected through NDVI, this is clear evidence of a colonisation process that resulted from
522 the pioneer vegetation of dunes (helped by experimental plantation during BEACHMED –Regione
523 Emilia Romagna “Foce Bevano: l’area naturale protetta e l’intervento di salvaguardia”). Vegetation
524 resilience may also have been favoured by the significant reduction of pumping water activities
525 from multi-layered aquifers (Fig. 4c).

526 The analysis of the EOF3 (explaining 2.5% of the total change) and its expansion coefficient show
527 an interesting trend that repeats following the same pattern within each decade (Figure 7c).

528 The change map shows how variations occurred in the coastal zone, with some pixels of riparian
529 vegetation along the river Bevano as well as in the river outlet that could be related to an impact of
530 groundwater salinity (Antonellini and Mollema, 2010).

531

532 **4.3 Trend analysis (EOFs)**

533 Based on the results highlighted above in the change detection for the whole time span, we
534 investigated the distribution of vegetation change phenomena at a higher temporal resolution (inside
535 each decade and/or in between the peaks detected from the empirical orthogonal functions).

536 In Foce Bevano, change detection was repeated for the two decades separately: for 1991-2001 and
537 2001-2010. In the first decade, it is evident that major losses in vegetation cover affected the outlet,
538 terminal stretch of the river, areas located behind the dunes and dunes and produced an overall loss
539 of 21% in vegetation cover in the whole image. These changes in vegetation confirm the strong
540 changes in the morphology of the river mouth and its rapid northern migration. The change
541 detection map of the second decade, however, shows a 9.7% increase in vegetation cover on the
542 dune system and river outlet; these findings may be explained by the stabilisation work carried out
543 in 2006, which was performed by re-vegetating the dunes to increase their stability (Figure 8) with

544 the objective of preventing further dune and beach loss. The change in scarce vegetation cover of
545 the dune system may, in fact, facilitate wave run-up flow and accelerate the washover
546 sedimentation processes (Sedrati et al., 2011).

547

548

549

550 *Figure 8 – SMA change detection in Foce Bevano between 2001–1991 (left) and 2010–2001 (right).*

551

552 **5. DISCUSSION**

553 The purpose of this study has been to identify phenomena and causes (natural and anthropogenic)
554 that contribute to a lowering of the topography of the Ravenna coastal area and Bevano River
555 mouth in particular, which experienced migration in the last decades. Subsequent to the intense
556 human activity in recent decades, the alarming situation has caused the public administration to
557 adopt new monitoring technique to manage the coastal subsidence. In areas where intense mining
558 activity (freshwater or hydrocarbons) occurs, the subsidence rates are higher than a metre per
559 century. The results obtained from the present study through the PSInSAR technique, indicate
560 increasing displacement rates after 1998 (approximately $-7 \div -9$ mm/year); before 1998, the velocity
561 was approximately $-3 \div -5$ mm/year in the 1992-1998 period, which is close to the values disclosed
562 by the ARPA-Emilia Romagna. The increase of settlement trends registered at the end of the 1990s
563 (Fig. 4c) is associated with the activation of gas extraction from the Angela-Angelina platform in
564 the "A.C27.EA" concession area.

565 Figure 9 shows the annual gas production from the A.C27.EA concession area, which is
566 characterised by offshore platforms located approximately 2 km from the coast (Angela Cluster and
567 Angela Angelina. The data were collected from the official website of the *Ministero dello Sviluppo*
568 *Economico of Italy* (UNMIG, <http://unmig.sviluppoeconomico.gov.it>). With reference to Fig. 9,
569 before 1997, the mean annual gas production was approximately 342 M Smc (data computed for the
570 1980-1996 period). After 1997, the Angela-Angelina platform was activated and a peak of gas
571 production occurred in 1998 (1,748 M Smc). After 2000, the production was gradually reduced and
572 in 2013, the values were close to those extracted before 1995 (approximately 400 m Smc).

573

574

575 *Figure 9 – Annual gas production from the A.C 27.EA concession area from 1980-2013 (data are taken from*
576 *the official website of the Ministero dello Sviluppo Economico of Italy (UNMIG,*
577 *<http://unmig.sviluppoeconomico.gov.it>).*

578 According to Gambolati (1998), the subsidence areas caused by the methane extraction from the
579 Angela-Angelina platform is manifested in a range of 4-5 km from the extraction field; therefore,
580 the study area may have been influenced by human activity. The subsidence trend registered in
581 1998 should have continued in the subsequent years, even after the drastic decrease of methane
582 extraction that has occurred since 2004: this aspect, which was highlighted by Baù et al. (2000),
583 represents a key point because the concession area should operate through 2027 at least. Because
584 the subsidence trend registered in recent years has not been as heavy as in past decades, the
585 reduction of gas field production and groundwater withdrawals suggests a stabilisation or slight
586 decrease of subsidence rates in the next decades, at least for those induced by human activities.

587 The overall results suggest that the presence of anthropogenic activities along the coast can strongly
588 affect natural subsidence dynamics and lead to subsidence phenomena with rates and timing almost
589 incomparable to the natural trends; therefore, a non-negligible effect on the coastal environment is
590 triggered. Specifically, the mouth of the river Bevano, which until 2005 was one of the few outlets
591 in the Emilia-Romagna coast that was not regimented by artificial embankments (Gardelli et al.,
592 2007) highlights numerous abandoned meanders near the beach within the time series analysis near
593 the outlet, with the last meander showing a marked northern migration that ran parallel to the coast.
594 The rapid migration that occurred in recent decades is mainly attributable to subsidence of the river
595 mouth, which can be seen from both analyses (PSInSAR and EOF techniques). The validity of the
596 data and results confirms that the subsidence rates obtained with SAR interferometry for the period
597 1992-2000 are consistent with the general subsidence trend in the Ravenna coastal area for both
598 natural and anthropogenic causes. In the mouth of the river Bevano, previous studies by Carminati
599 and Martinelli (2002) and Teatini et al. (2005) recorded a total subsidence of 90 cm from 1897 to
600 1992, which was based on geometric levelling data derived from IGM campaigns. In particular,
601 subsidence peaks were found between 1950 and 1980 in which both methane extraction and water
602 withdrawal occurred (Carminati and Martinelli, 2002). After this date, the reduction of groundwater
603 extraction led to a significant decrease of subsidence rates. As shown in Fig. 4c and Fig. 9, when
604 the groundwater extraction was reduced (potentiometric surface gradually recovered from the
605 1980s) an increase in natural gas extraction occurred in August 1998. Because of several appeals in
606 2004, a gradual decrease in gas production was observed. The displacement time series between
607 1992 and 2010 indicated a land subsidence of approximately 80 mm. The mean velocities
608 synthetically represent the general pattern of ground deformation; however, the time series exhibits
609 nonlinear components shown by the change of slope, which is indicative of the presence of different
610 linear trends (Fig. 4c). Two distinct trends can be identified; from 1992 to 1999, the displacement
611 was limited to less than 20 mm and could be related by both natural and anthropogenic causes

612 (Bertoni et al., 2005) and from August 1998, a steeper slope indicated a faster displacement that
613 resulted from the contemporary beginning of methane extraction in the “Angela-Angelina” platform
614 (4 km NE of Foce Bevano). Despite the reduction in gas extraction starting in 2004 (Fig. 9) and the
615 recovery of potentiometric surface as a result of the stoppage of pumping wells, the displacements
616 remained roughly the same from 1998 to 2010 (approximately -9 mm/year). In general, the
617 displacement rates appear to have reached high values that were not as high as the values registered
618 in the past when both the groundwater and gas extractions were operating. According to Teatini et
619 al. (2005), from 1972-1977, a subsidence rate of approximately -45 mm/year was registered in the
620 Bevano area according to levelling surveys.

621 In addition, our multi-temporal analysis shows that for a given location with high subsidence rates,
622 the surrounding area shows vegetation losses consistent with the negative evolution of the coastal
623 stretch. Most of these locations correspond to areas subject to anthropic pressure and show a high
624 correlation with pumping activities that exacerbated the subsidence problem. At these sites, 9% of
625 the loss in vegetation represents a threshold value to delineate the signature of vegetation loss
626 within the subsidence pixels. There is also a correspondence between the peaks in the first two
627 EOFs (Figure 7b and c) and main trends in the displacement time series (Figure 4c). The two
628 vegetation peaks in 1998 and 2004 for EOF1 and EOF2, respectively, may represent the
629 vegetation’s response to the impacts of a faster subsidence trend, which re-started in 1998 likely as
630 a result of the increase in methane extraction. The results compared with previous studies highlight
631 that both the depth of the water table from the surface and water salinity are very important factors
632 in controlling vegetation distribution, with a high density where the water table is deep
633 (approximately 1.5 m or more) and salinity is low (Antonellini and Mollema, 2010). These
634 measurements in the dune slacks and estuaries indicate a significant relationship between salinity
635 degree, vegetation species richness and subsidence rates. A decrease in plant species richness and
636 density occurs in the coastal vegetation when a subsidence rate threshold is exceeded (-6 mm/year).
637 Results show that a generally small loss of vegetation has been observed. However, a decrease in
638 the total vegetation amount was observed, and this is the opposite of the change expected based on
639 its relation with elevation (an increase). Management of the vegetation presence will thus need to
640 take into account each of these factors, based on specific habitat and species richness conservation
641 objectives dealing with extreme event. Wetland reclamation, groundwater pumping for agricultural
642 and industrial purposes, and methane extraction near the coast are among the main causes of
643 anthropogenic subsidence (Van Dobben and Slim; 2012; Chaussard et al., 2013). The coastal area
644 could be particularly impacted by accelerated subsidence, which often results in higher flooding
645 frequencies in low-lying areas. The work conducted on the dune system between Lido di Dante and

646 Foce Bevano has detected a general degradation of the dunes between 2001 and 2009 (Ciavola and
647 Armaroli, 2010; Sedrati et al., 2011; Armaroli et al., 2012). Across this period, an exceptional storm
648 occurred in September 2004, which triggered an erosion phase not compensated according to
649 Gardelli et al. (2007) that was not balanced by sediment injection through replenishments, which
650 could explain some of the patterns observed in the first and second-order EOF components.

651

652

653 **6 CONCLUSIONS**

654 This research shows that remote sensing methods are effective in analysing variability and the
655 resulting uncertainties in several parameters of relevance to flooding. The feedback between the
656 climatological, biophysical and morphological parameters illustrated here are not only conceptual
657 but are one of the first attempts to quantitatively evaluate different physically remote sensing-based
658 models at a local to regional scale. The results emphasise that using hierarchical remote sensing
659 vegetation pattern models over time can demonstrate how the morphology of different subsystems
660 represent a balance between inputs (forcing agents such as climate) and natural responses (related
661 single changes such as vegetation evolution). Moreover, the temporal evolution morphology (e.g.,
662 subsidence rate) also influences the temporal evolution produced by the different vegetation
663 parameters identified for the study sites. Considering the extrapolation of the historical trends
664 shown by the different approaches, the possible future evolution including uncertainties, are
665 highlighted. The PSInSAR technique may be a useful tool for the Authority in charge for the
666 management of the land subsidence to check preliminarily, in the case of a possible further request
667 of the extension of the concession licence, the critical withdrawal in terms of expected anthropic
668 subsidence and its effect on coastal area. Moreover, the analysis of subsidence trend allows to
669 understanding the response time between the increase of methane withdrawals and the acceleration
670 and magnitude of subsidence rates. This approach, coupled with the fact that recent Italian law (DM
671 9 Agosto 2013) does not allow the exploration and exploitation of new gas fields under 12 miles
672 from the coastline, may be considered a key instrument to limit further geomorphological and
673 environmental problems along the northern Adriatic coast. The considerations here obtained may be
674 of such utility to understand and to manage the effects, which can be triggered in geologically
675 similar area, affected by heavy groundwater and methane extractions. Therefore, we suggest that
676 the ground velocity subsidence rate maps obtained using DInSAR techniques and integrated to the
677 multispectral endmember fraction maps can provide a quantitative parameter to improve the
678 monitoring approach for coastal areas. Being the observations by PSInSAR technique acquired at
679 about monthly scale over extensive areas, the subsidence phenomenon can be evaluated step by step

680 relating it with vegetation variation and changes. The occurrence of soil subsidence in coastal areas
681 can be used then as a case study to mimic sea level rise and its effects on vegetation. The Bevano
682 test area represents an ideal test case because of substantial coastal estuary areas and subsidence due
683 to water pumping and gas extraction activities.

684

685 **ACKNOWLEDGEMENTS**

686 The support of the European Commission through the projects THESEUS (Contract 244104) and
687 MICORE (Contract 202798) are gratefully acknowledged. Permanent Scatter data were from the
688 PROGETTO PSI: Progetto Persistent Scatterers Interferometry (PSI) Ministero dell'Ambiente-
689 Portale cartografico Nazionale (http://www.pcn.minambiente.it/GN/progetto_psi.php?lan=it#).
690 Data provided by the European Space Agency and USGS.

691

692 **REFERENCES**

- 693 Antonellini, M., Mollema, P., 2010. Impact of groundwater salinity on vegetation species richness
694 in the coastal pine forests and wetlands of Ravenna, Italy. *Ecological Engineering*. 36, 1201–
695 1211.
- 696 Armaroli, C., Ciavola, P., Perini, L., Lorito, S., Valentini, A., Masina, M., 2012. Critical storm
697 thresholds for significant morphological changes and damage along the Emilia-Romagna
698 coastline, Italy. *Geomorphology* 143–144, 34–51.
- 699 Armaroli, C., Grottoli, E., Harley, M.D., Ciavola, P., 2013. Beach morphodynamics and types of
700 foredune erosion generated by storms along the Emilia-Romagna coastline, Italy.
701 *Geomorphology*. 199, 22-35.
- 702 AQUATER, 1988. Caratteristiche idrogeologiche, idrauliche ed idrodinamiche della falda freatica e
703 rapporti falda freatica-subsidenza nelle pinete di S. Vitale e di classe (RA). Comune di
704 Ravenna (Italy). Technical Report (in italian).
- 705 Balouin, Y., Ciavola, P., Michel, D., 2006. Support of subtidal tracer studies to quantify the
706 complex morphodynamics of a river outlet: the Bevano, NE Italy. *J Coastal Res.* SI 39: 602-
707 607.
- 708 Bamler, R., Hartl, P., 1998. Synthetic aperture radar interferometry. *Inverse Probl.* 14:R1-R54.
- 709 Baù, D., Gambolati, G., Teatini, P., 2000. Residual land subsidence near abandoned gas fields
710 raises concern over Northern Adriatic Coastland. *EOS, Transaction, American Geophysical*
711 *Union*. 81, 245–252.

- 712 Berardino, P., Fornaro, G., Lanari, R. and Sansosti, E., 2002. A new algorithm for surface
713 deformation monitoring based on small baseline differential SAR interferograms. *IEEE Trans.*
714 *Geosci. Remote Sen.* 40(11): 2375-238.
- 715 Bertoni, W., Elmi, C., Marabini, F., 2005. The subsidence of Ravenna. *Giornale di Geologia*
716 *Applicata.* 1, 23–32.
- 717 Bjornsson, H., Venegas, S., 1997. A manual for EOF and SVD analyses of climatic data. CCGCR
718 Report, 97(1).
- 719 Boardman, W.J., 1989. Inversion of imaging spectrometry data using singular value decomposition.
720 *Proceedings of the 12th Canadian Symposium on remote sensing*, pp. 2069-2072.
- 721 Bock, Y., Wdowinski, S., Ferretti, A., Novali, F., Fumagalli, A. 2012. Recent subsidence of the
722 Venice Lagoon from continuous GPS and interferometric synthetic aperture radar.
723 *Geochemistry Geophysics Geosystems.* 13(3), Q08011, doi:10.1029/2012GC004270.
- 724 Bürgmann, R., Rosen, P.A. and Fielding, E.J., 2000. Synthetic aperture radar interferometry to
725 measure Earth's surface topography and its deformation. *Annu Rev Earth Pl Sc.* 28(1), 169-
726 209.
- 727 Cahoon, D. R., Reed, D.J., Day, J.W., 1995. Estimating shallow subsidence in microtidal salt
728 marshes of the southeastern United States: Kaye and Barghoorn revisited. *Mar Geol.* 128:1-9.
- 729 Carbognin, L., Tosi, L., 2003. Il progetto ISES per l'analisi dei processi di intrusione salina e
730 subsidenza nei territori meridionali delle province di Padova e Venezia. Istituto per lo Studio
731 della Dinamica delle Grandi Masse e Consiglio Nazionale delle Ricerche. Venezia (Italy). 63–
732 83.
- 733 Carminati, E., Martinelli, G., 2002. Subsidence rates in the Po Plain, northern Italy: the relative
734 impact of natural and anthropogenic causation. *Eng Geol.* 66, 241–255.
- 735 Cernica, J.N., 1995. *Geotechnical engineering: soil mechanics.* Wiley, New York.
- 736 Chander, G., Markham, B. L., 2003. Revised Landsat-5 TM radiometric calibration procedures, and
737 post-calibration dynamic ranges. *IEEE Trans. Geosci. Remote Sen.* 41, 2674–2677.
- 738 Chander, G., B. Markham, and D. Helder, 2009. Summary of current radiometric calibration
739 coefficients for Landsat MSS, TM, ETM+, and EO-1 ALI sensors. *Remote Sensing of the*
740 *Environment*, 113: 893-903.
- 741 Chaussard, E., Falk Amelung, F., Abidin, H., Hong S-H., 2013. Sinking cities in Indonesia: ALOS
742 PALSAR detects rapid subsidence due to groundwater and gas extraction. *Remote Sens*
743 *Environ.* 128, 150–161.
- 744 Chen, Z., Rybczyk, J., 2005. Coastal Subsidence. In: Schwartz, M. (ed.), *Encyclopedia of Coastal*
745 *Science.* Springer Academic Publishers, Netherlands, pp. 302–304.

746 Ciavola, P., Armaroli, C., 2010. Evoluzione recente del sistema dunale di Lido di Dante-Foce
747 Bevano (Ravenna): fattori naturali ed impatto antropico. *Studi Costieri*. 17, 19–38 (in Italian).

748 Ciavola P., Armaroli C., Chiggiato J., Valentini A., Deserti M., Perini L., Luciani P. (2007). Impact
749 of storms along the coastline of Emilia-Romagna: the morphological signature on the Ravenna
750 coastline (Italy): *Journal of Coastal Research SI 50* : 540-544.

751 Ciavola P., Tondello M., Carniel S., and Sclavo M. (2012). Artificial deviation of a small inlet
752 (Bevano, northern Italy): prediction of future evolution and planning of management strategies
753 using open-source community coastal models. *Coastal Engineering Proceedings*, 1(33),
754 management.57. doi:10.9753/icce.v33.management.57

755 Cibin, U., Severi, P., Correggiari, A., Roveri, M., et al. 2005. Note illustrative della carta geologica
756 d'Italia alla scala 1:50.000 - Foglio 240-241 Forlì-Cervia. APAT (Agenzia per la Protezione
757 dell'Ambiente e per i servizi Tecnici), Dipartimento Difesa del Suolo, Servizio Geologico
758 Italiano. pp 104.

759 Coppin, P., Jonckheere, I., Nackaerts, K., Muys, B. and Lambin, E., 2004. Digital change detection
760 methods in ecosystem monitoring: a review. *Int J Remote Sens*. 25(9), 1565-1596.

761 Corenblit, D., Baas, A.C.W., Bornette, G., Darrozes, J., Delmotte, S., Francis, R.A., Gurnell, A.M.,
762 Julien, F., Naiman, R.J., Steiger, J., 2011. Feedbacks between geomorphology and biota
763 controlling Earth surface processes and landforms: A review of foundation concepts and
764 current understandings. *Earth Sci*. 106, 307–331.

765 Correggiari, A., Cattaneo, A. Trincardi, F., 2005, The modern Po Delta system: Lobe switching and
766 asymmetric prodelta growth", *Marine Geology*, 222-223, 1-4, 49-74.

767 D'Alpaos, A., Da Lio, C., Marani M., 2012. Biogeomorphology of tidal landforms: physical and
768 biological processes shaping the tidal landscape. *Ecology*. 5, 550–562.

769 Domenico, A., Schwartz, F.W., 1998. *Physical and chemical hydrology*, 2nd edn. Wiley, New
770 York.

771 Evans, E., Ashley, R., Hall, J., Penning-Rowsell, E., Saul, A., Sayers, P., Thorne, C., Watkinson,
772 A., 2004. *Foresight: Future Flooding. Scientific Summary. Volume I - Future risks and their
773 drivers*. London, UK; Office of Science and Technology (OST).

774 Farr, T.G., Rosen, P.A., Caro, E., Crippen, R., Duren, R., Hensley, S., Kobrick, M., Paller, M.,
775 Rodriguez, E. and Roth, L., 2007. The shuttle radar topography mission. *Rev of Geophys*.
776 45(2), 33.

777 Ferretti, A., Prati, C., Rocca, F., 2001. Permanent scatterers in SAR interferometry. *IEEE Trans*.
778 *Geosci. Remote Sens*. 39, 8 – 20.

779 Galloway, D., Jones D.R., Ingebritsen, S.E., 1999. Land Subsidence in the United States. U.S.
780 Department of the Interior and U.S. Geological Survey. Circular 1182, 177.

781 Gambolati, G., 1998. CENAS: Coastline Evolution of the Upper Adriatic Sea due to Sea Level Rise
782 and Natural and Anthropogenic Land Subsidence. Kluwer Academic Publishers. Dordrecht,
783 pp. 344.

784 Gardelli, M., Caleffi, S., Ciavola, P., 2007. Evoluzione morfodinamica della foce del Torrente
785 Bevano. Studi Costieri. 13, 53–74.

786 Goward, S.N., Markham, B., Dye, D.G., Dulaney, W. and Yang, A.J., 1991. Normalized difference
787 vegetation index measurements from the Advanced Very High Resolution Radiometer. Remote
788 Sens Environ. 35, 257-277.

789 Hallegate, S., Green, C., Nicholls, R.J. and Corfee-Morlot, J., 2013. Future flood losses in major
790 coastal cities. Nature Climate Change. 3, 802–806.

791 Hannachi, A., Jolliffe, I., Stephenson, D., 2007. Empirical orthogonal functions and related
792 techniques in atmospheric science: A review. Int J Climatol. 27(9), 1119-1152.

793 Hanssen, R.F., 2001. Radar interferometry: data interpretation and error analysis, 2. Kluwer
794 Academic Pub.

795 Hung, W.-C., Hwang, C., Chang, C.-P., Yen, J.-Y., Liu, C.-H., Yang, W.-H., 2010. Monitoring
796 severe aquifer-system compaction and land subsidence in Taiwan using multiple sensors:
797 Yunlin, the southern Choshui River Alluvial Fan. Environmental Earth Sciences. 59 (7), 1535–
798 1548.

799 Kerr, J.T., Ostrovsky, M., 2003. From space to species: ecological applications for remote sensing.
800 Trends Ecol Evol. 18(6), 299-305.

801 ITER, 1989. Progetto esecutivo per l'adeguamento della discarica provinciale ai sensi dell'art. 1 del
802 D.L. 36/87 e alle disposizioni del D.P.R. 915/82. Technical Report (in italian).

803 Jacob, C.E., 1940. On the flow of water in an elastic artesian aquifer. Trans. Am. Geophys. Union.
804 22, 574–586.

805 Lanari, R.; Mora, O.; Manunta, M.; Mallorqui, J.; Berardino, P.; Sansosti, E., 2004. A small-
806 baseline approach for investigating deformations on full-resolution differential SAR
807 interferograms Geoscience and Remote Sensing, IEEE Transactions, 42, 1377-1386.

808 Lorenz, E.N., 1956. Empirical orthogonal functions and statistical weather prediction, Report no.1,
809 Statistical forecasting project, MIT Massachusetts Institute of Technology, Department of
810 Meteorology, Cambridge, Massachusetts.

811 Lu, D., Mausel, P., Brondizio, E. and Moran, E., 2004. Change detection techniques. Int J Remote
812 Sens. 25(12), 2365-2401.

813 Marani, M., Belluco, E., Ferrari, S., Silvestri, S., D'Alpaos, A., Lanzoni, S., Feola, A., Rinaldo A.,
814 2006. Analysis, synthesis and modelling of high-resolution observations of salt-marsh
815 ecogeomorphological patterns in the Venice lagoon. *Estuar Coast Shelf S.* 69, 414–426.

816 Marani, M., D'Alpaos, A., Lanzoni, S., Carniello, L., Rinaldo, A., 2010. The importance of being
817 coupled: Stable states and catastrophic shifts in tidal biomorphodynamics. *J Geophys Res.* 115.

818 Marquenie, JP., de Vlas, J., 2005, The impact of subsidence and sea level rise in the Wadden Sea:
819 prediction and field verification, in J.E. Vermaat et al., (Eds.): *Managing European Coasts:
820 Past, Present and Future*, Springer Verlag Berlin Heidelberg 2005, pp. 355-363.

821 Massonnet, D., Feigl, K.L., 1998. Radar interferometry and its application to changes in the Earth's
822 surface. *Rev of Geophys.* 36(4), 441-500.

823 MATTM, 2009. Linee guida per l'analisi di dati interferometrici satellitari in aree soggette a
824 dissesti idrogeologici. Ministero dell'Ambiente e della Tutela del Territorio e del Mare. Piano
825 Straordinario di Telerilevamento Ambientale (PST-A), lotto 2.

826 Meinzer, O.E. 1928. Compressibility and elasticity of artesian aquifers. *Econ. Geol.* 23, 263–291.

827 Nicholls, R.J., Marinova, M., Lowe, J.A., Brown, S., Vellinga, P., De Gusmao, D., Hinkel, J., Tol,
828 R.S.J., 2011. Sea-level rise and its possible impacts given a 'beyond 4°C world' in the twenty-
829 first century. *Philosophical Transactions of the Royal Society A-mathematical Physical and
830 Engineering Sciences.* 369, 161–181.

831 Passalacqua, P., Lanzoni, S., Paola, C., Rinaldo, A., 2013. Geomorphic signatures of deltaic
832 processes and vegetation: The Ganges-Brahmaputra-Jamuna case study. *Journal of
833 Geophysical Research: Earth Surface.* 118, 1–12.

834 Pettorelli, N., Vik, J.O., Mysterud, A., Gaillard, J.-M., Tucker, C.J. and Stenseth, N.C., 2005. Using
835 the satellite-derived NDVI to assess ecological responses to environmental change. *Trends
836 Ecol Evol.* 20(9), 503-510.

837 Pimm, S. L., 1984. The complexity and stability of ecosystems. *Nature.* 307, 321–326.

838 Poland, J.F., 1984. Guidebook to studies of land subsidence due to ground-water withdrawal: v. 40
839 of UNESCO Studies and Reports in Hydrology: Paris, France, United Nations Educational,
840 Scientific and Cultural Organization, 305 pp.

841 Reinhardt, L., Jerolmack, D., Cardinale, B.J., Vanacker, V., Wrigh, J., 2010. Dynamic interactions
842 of life and its landscape: feedbacks at the interface of geomorphology and ecology. *Earth Surf.
843 Process. Landforms.* 35, 78–101.

844 RER and ENI-AGIP, 1998. Riserve idriche sotterranee nella Regione Emilia-Romagna. Di Dio G.
845 (Ed.), 119 pp., 9 sheets, S.EL.CA., Firenze.

846 Ricci Lucchi, F., Colalongo, M.L., Cremonini, G., Gasperi, G.F., Iaccarino, S., Papani, G., Raffi, S.,
847 Rio, D., 1982. Evoluzione sedimentaria paleogeografica nel margine appenninico. Guida alla
848 geologia del margine appenninico padano. Guide Geologiche Regionali. S.G.I. 17–46.

849 Rosen, P., Hensley, S., Joughin, I., Li, F., Madsen, S., Rodríguez, E., Goldstein, R., 2000. Synthetic
850 aperture radar interferometry. *Proc. of the IEEE*. 88(3): 333-382.

851 Sedrati, M., Ciavola, P., Armaroli, C., 2011, Morphodynamic evolution of a microtidal barrier; the
852 role of overwash: Bevano, Northern Adriatic Sea, *Journal of Coastal Research*, vol. SI 64, p.
853 696-700, ISSN: 0749-0208.

854 Singh, A., 1989. Digital change detection techniques using remotely-sensed data. *Int J Remote*
855 *Sens.* 10(6), 989-1003.

856 Small, C., 2004. The Landsat ETM+ spectral mixing space. *Remote Sens Environ.* 1-2(93), 1-17.

857 Strozzi, T., Wegm, U., Werner, C., Wiesmann, A., Spreckel, V., 2003, JERS SAR interferometry
858 for land subsidence monitoring, *IEEE Trans. Geosci. Remote Sensing*, 41, 7, 1702 - 1708.

859 Sun, H., Grandstaff, D., Shagam, R., 1999. Land subsidence due to groundwater withdrawal:
860 potential damage of subsidence and sea level rise in southern New Jersey, USA. *Environ Geol.*
861 37, 290–296.

862 Syvitski, J.P.M., Kettner, A.J., Overeem, I., Hutton, E.W.H., Hannon, M.T., Brakenridge, G.R.,
863 Day, J., Vörösmarty, C., Saito, Y., Giosan, L., Nicholls R.J., 2009. Sinking deltas due to
864 human activities. *Nat Geosci.* 2, 681–686.

865 Taramelli, A., Valentini, E., Dejana, M., Zucca, F., Mandrone, S., 2011. Modelling coastal
866 processes by means of innovative integration of remote sensing time series analysis. In: *Proc.*
867 *of Geoscience and Remote Sensing Symposium (IGARSS)*, 2011 IEEE International,
868 Vancouver, BC, pp. 1547-1550. (DOI 10.1109/IGARSS.2011.6049364).

869 Taramelli, A., Valentini, E., Cornacchia, L., Mandrone, S., Monbaliu, J., Thompson, R., Hogart, S.,
870 Zanuttigh, B., 2013a. Modelling uncertainty in estuarine system by means of combined
871 approach of optical and radar remote sensing. *Coast Eng.*, 87, 77-96.
872 10.1016/j.coastaleng.2013.11.001.

873 Taramelli, A., Pasqui, M., J. Barbour, D. Kirschbaum, L. Bottai, C. Busillo, F. Calastrini, Guarnieri,
874 F., Small, C., 2013b. Spatial and temporal dust source in Northern China identified using
875 advanced remote sensing analysis. *Earth Surf Proc and Land.* 38, 793–809.

876 Taramelli, A., Manzo, C., Valentini, E., Cornacchia, L., Pieralice, F., 2014a. Coastal Subsidence:
877 Causes, Mapping and Monitoring. Invited Chapter to *Encyclopedia of Natural Hazards*.
878 Wiley&Sons, Ltd. In press.

879 Taramelli, A., Cornacchia, L., Valentini, E., Bozzeda, F., 2014b. Non-linear power law approach
880 for spatial and temporal pattern analysis of salt marsh evolution. *Earth Surf. Dynam. Discuss.*
881 1, 1061-1095, DOI:10.5194/esurfd-1-1061-2013.

882 Teatini, P., Ferronato, M., Gambolati, G., Bertoni, W., Gonella, M., 2005. A century of land
883 subsidence in Ravenna, Italy. *Environ Geol.* 47, 831–846.

884 Temmerman, S., Bouma, T.J., Van de Koppel, J., Van der Wal, D., De Vries, M.B., Herman,
885 P.M.J., 2007. Vegetation causes channel erosion in a tidal landscape. *Geology.* 35, 631–634.

886 Temmerman, S., Govers, G., Wartel, S., Meire, P., 2003. Spatial and temporal factors controlling
887 short-term sedimentation in a salt and freshwater tidal marsh, Scheldt estuary, Belgium, SW
888 Netherlands. *Earth Surf Proc Land.* 28, 739–755.

889 Tolomei, C., Taramelli, A., Moro, M., Saroli, M., Salvi, S., 2013. Analysis of DGSD impending
890 over the Fiastra lake (Central Italy), by geomorphological assessment and deformation
891 monitoring using satellite SAR Interferometry, *Geomorphology.* 201, 281-292.

892 Tosi, L., Teatini, P., Carbognin, L., Brancolini, G., 2009. Using high-resolution data to reveal
893 depth-dependent mechanisms that drive land subsidence; the Venice coast, Italy.
894 *Tectonophysics.* 474 (1–2), 271–284.

895 Tosi, L., Teatini, P., Bincoletto, L., Simonini, P., Strozzi, T., 2012. Integrating geotechnical and
896 interferometric SAR measurements for secondary compressibility characterization of coastal
897 soils. *Surv. Geophys.* 33, 907–926.

898 Tosi, L., Teatini, P., Strozzi, T., 2013. Natural versus anthropogenic subsidence of Venice. *Sci.*
899 *Rep.* 3, 2710; DOI:10.1038/srep02710.

900 T.R.E., 2008. *Tele-Rilevamento Europa. PSInSARTM – Manuale d’uso.*

901 Van Dobben, H.F., Slim, P.A., 2012. Past and future plant diversity of a coastal wetland driven by
902 soil subsidence and climate change. *Climatic Change.* 110(3-4), 597-618.

903 Van Dobben, H.F., Slim P.A., 2005, Evaluation of changes in permanent plots in the dunes and
904 upper salt marsh at Ameland East: ecological effects of gas extraction. In:
905 *Begeleidingscommissie Monitoring Bodemdaling Ameland (ed) Monitoring effecten van*
906 *bodemdaling op Ameland-Oost*, 1–36.

907 Van Wesenbeeck, B.K., Van de Koppel, J., Herman, P.M.J., Bouma, T.J., 2008. Does scale-
908 dependent feedback explain spatial complexity in salt-marsh ecosystems?. *Oikos.* 117, 152–
909 159.

910 Zebker, H.; Villasenor, J., 1992. Decorrelation in interferometric radar echoes *Geoscience and*
911 *Remote Sensing, IEEE Transactions on,* 30, 950-959.

912 Zurlini, G., Riitters, K., Zaccarelli, N., Petrosillo, I., Jones, K., Rossi, L., 2006a. Disturbance
913 patterns in a socio-ecological system at multiple scales. *Ecol Complex.* 3(2), 119-128.

914 Zurlini, G., Zaccarelli, N., Petrosillo, I., 2006b. Indicating retrospective resilience of multi-scale
915 patterns of real habitats in a landscape. *Ecol Indic.* 6, 184-204.

916 Wang, C., Temmerman, S., 2013. Does biogeomorphic feedback lead to abrupt shifts between
917 alternative landscape states: An empirical study on intertidal flats and marshes. *Journal of*
918 *Geophysical Research. Earth Surface.* 118, 229–240.

919

920

921

922

923 TABLES

924

925 *Table I: Specifications of the Landsat Enhanced Thematic Mapper (ETM+) sensor (U.S.*
926 *Geological Survey, 2003).*

Band n.	Wavelength (µm)	Spatial resolution (m)
1	0.45 - 0.515	30
2	0.525 - 0.605	30
3	0.63 - 0.69	30
4	0.75 - 0.90	30
5	1.55 - 1.75	30
6	10.4 - 12.5	60
7	2.09 - 2.35	30
8	0.52 - 0.9	15

927

Acquisition date	Sensor	Path	Row
07/08/1991	TM	192	29
24/07/1992	TM	192	29
04/07/1993	TM	191	29
14/07/1994	TM	192	29
01/07/1995	TM	192	29
01/06/1996	TM	192	29
22/07/1997	TM	192	29
18/07/1998	TM	191	29
13/07/1999	ETM	191	29
20/06/2000	ETM	192	29
03/08/2001	ETM	191	29
27/06/2002	TM	192	29
16/07/2003	TM	191	29
18/07/2004	TM	191	29
10/06/2005	TM	192	29
01/09/2006	TM	192	29
27/07/2007	TM	191	29
29/07/2008	TM	191	29
16/07/2009	TM	191	29
03/07/2010	TM	191	29
27/06/2011	TM	192	29

933 *Table 3 –Specifications of the ERS sensors*

Satellite	ERS-1	ERS-2
Launch date	17 July 1991	21 April 1995
Altitude	800 Km	800 Km
Revisiting cycle	35 days	35 days
Acquisition time	21.16 in ascending orbit 9.40 in descending orbit	21.16 in ascending orbit 9.40 in descending orbit
Orbit inclination	98.5 degree inclination orbit	98.5 degree inclination orbit
Look angle	23 deg look angle towards right	23 deg look angle towards right
Band/wavelength	C/5.8 cm	C/5.8 cm
Frame Dimension	100x100 Km	100x100 Km
SAR pixel size	12.5x12.5 m (3 looks)	12.5x12.5 m (3 looks)

ERS-1/2 SAR	
10/05/1992	02/07/1997
14/06/1992	06/08/1997
27/09/1992	15/10/1997
01/11/1992	08/04/1998
06/12/1992	13/05/1998
21/03/1993	17/06/1998
25/04/1993	22/07/1998
12/09/1993	26/08/1998
21/11/1993	30/09/1998
02/08/1995	24/03/1999
10/10/1995	28/04/1999
28/02/1996	02/06/1999
02/04/1996	06/07/1999
07/05/1996	07/07/1999
08/01/1997	15/09/1999
12/02/1997	20/10/1999
23/04/1997	24/11/1999
28/05/1997	29/12/1999

Figure1
[Click here to download high resolution image](#)

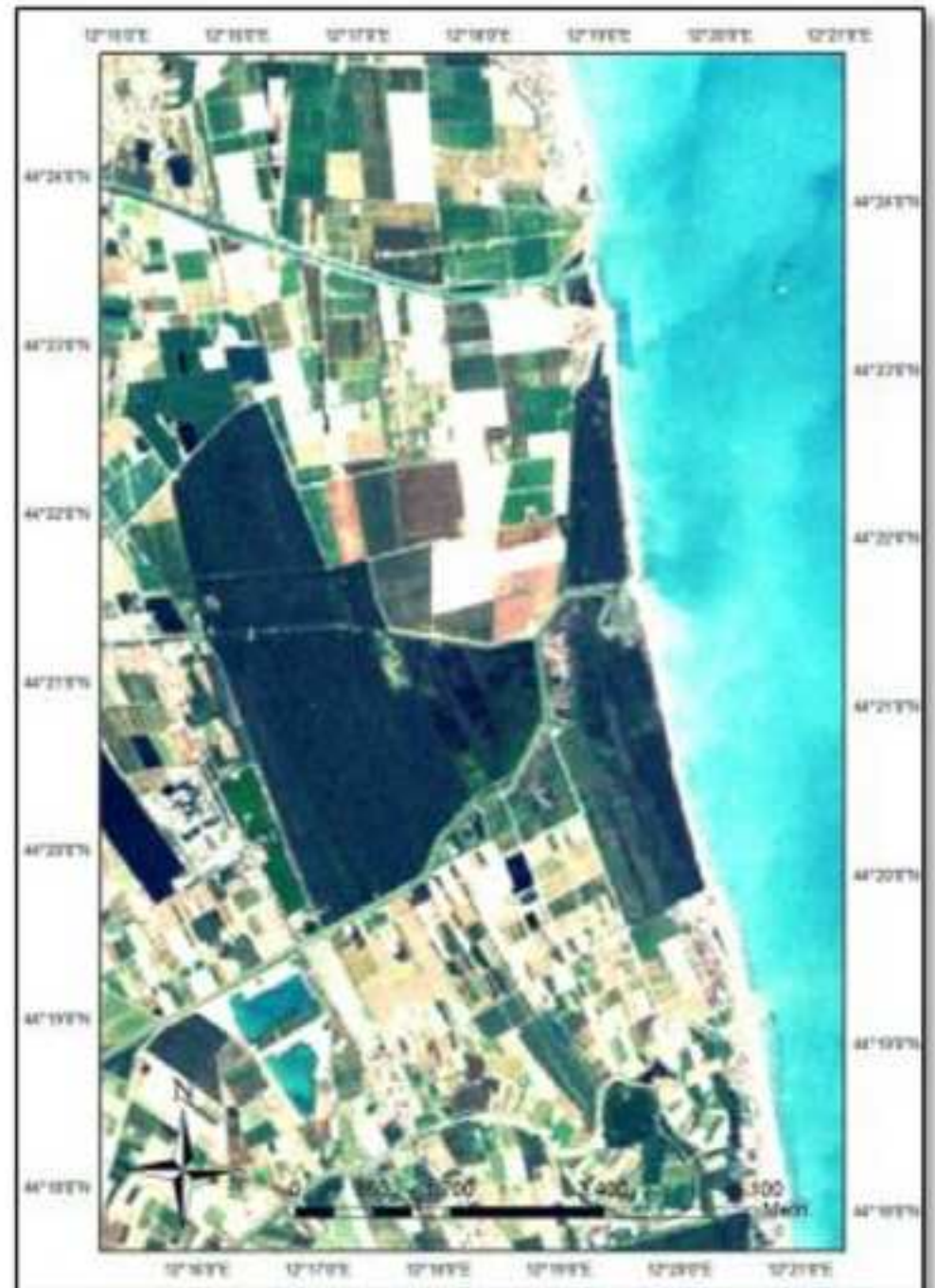
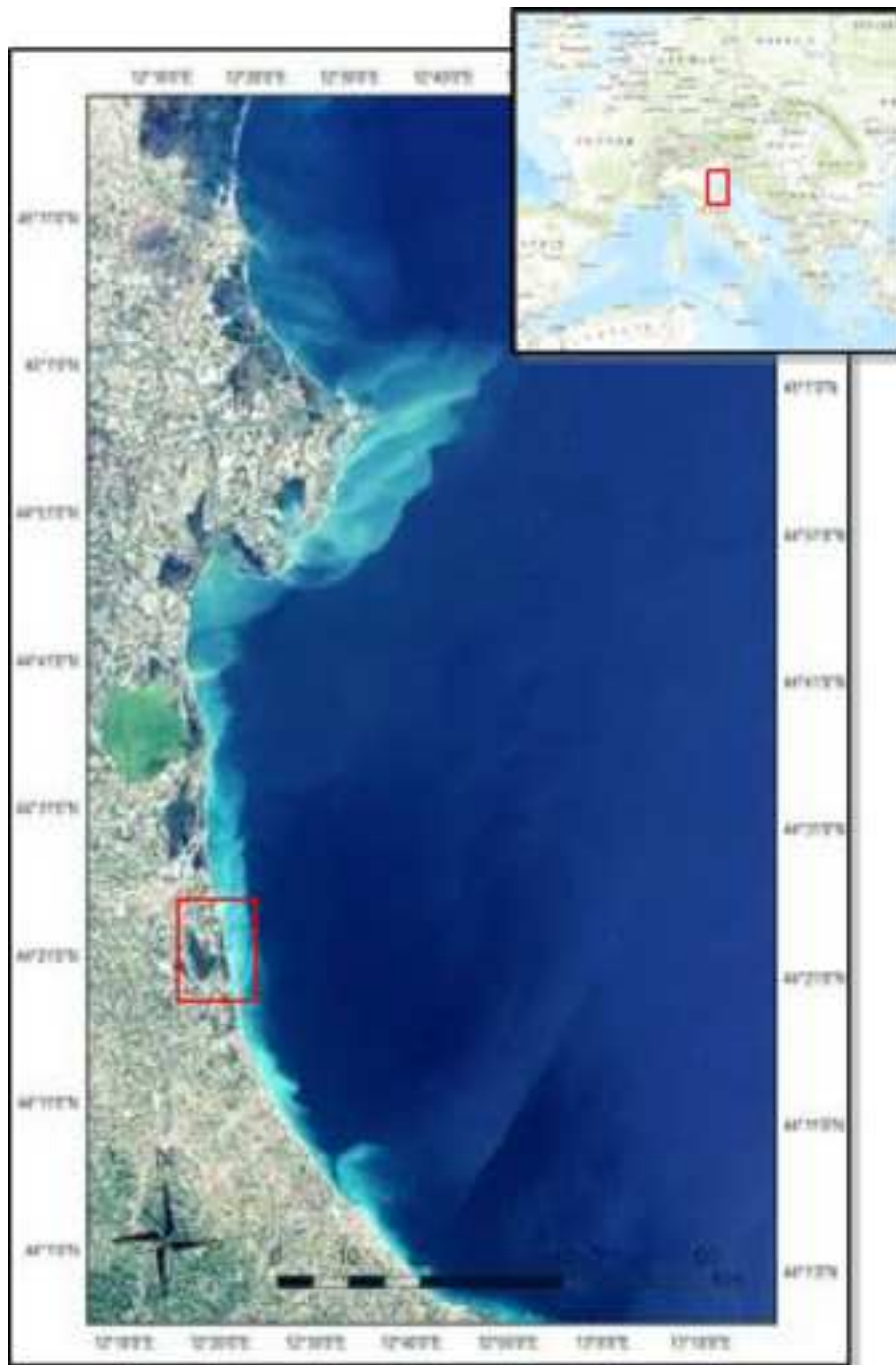


Figure2

[Click here to download high resolution image](#)

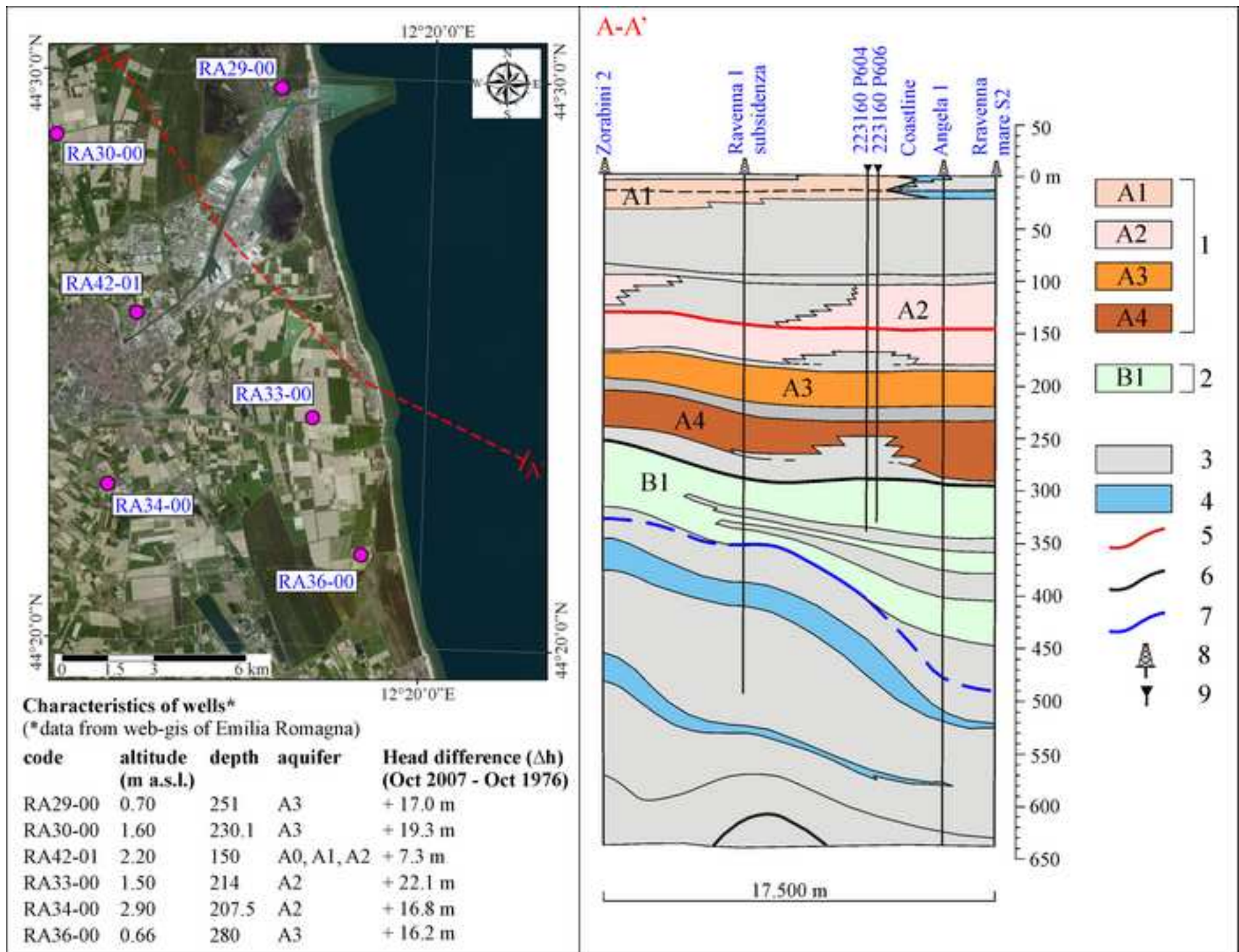
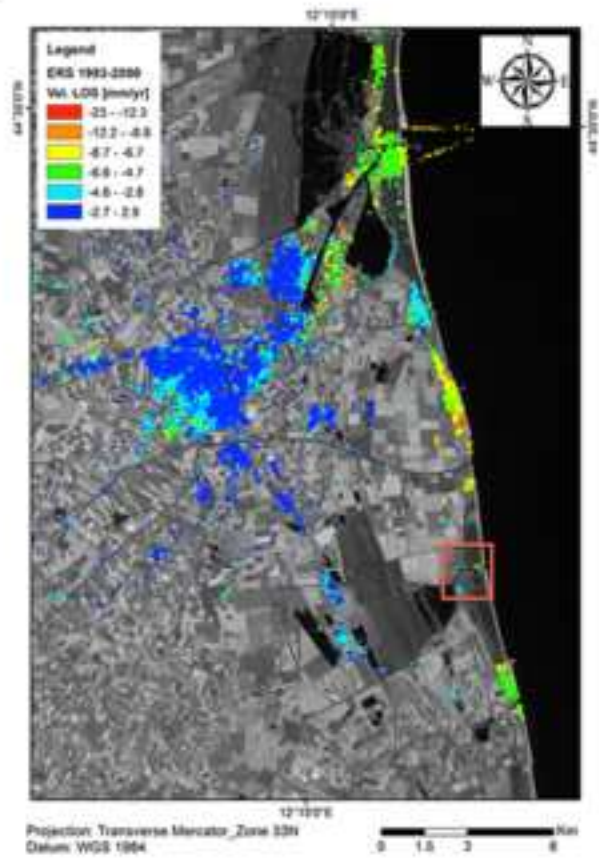


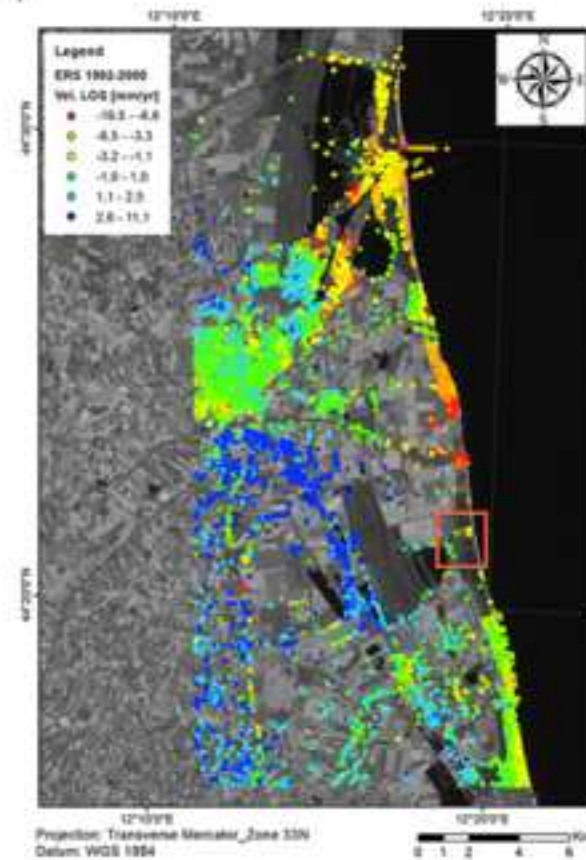
Figure3

[Click here to download high resolution image](#)

a)



b)



c)

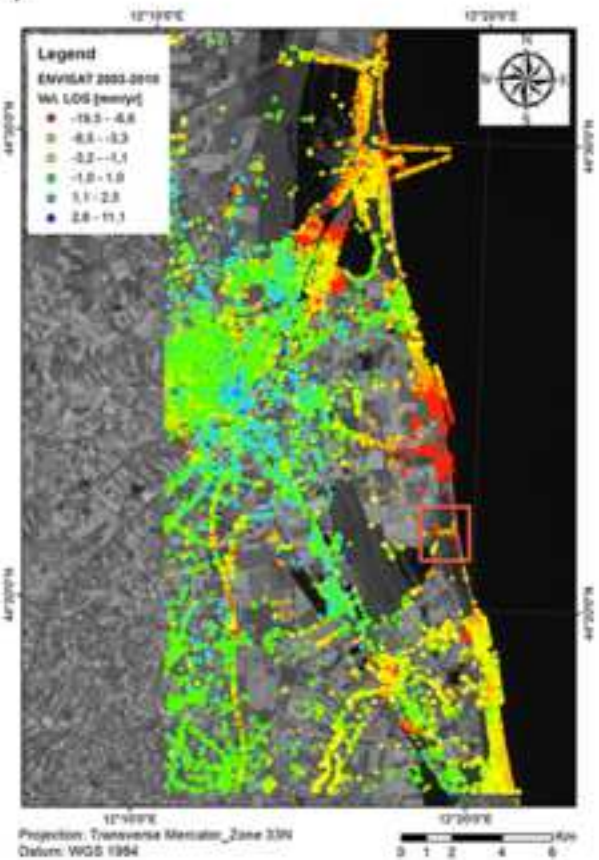


Figure4
[Click here to download high resolution image](#)

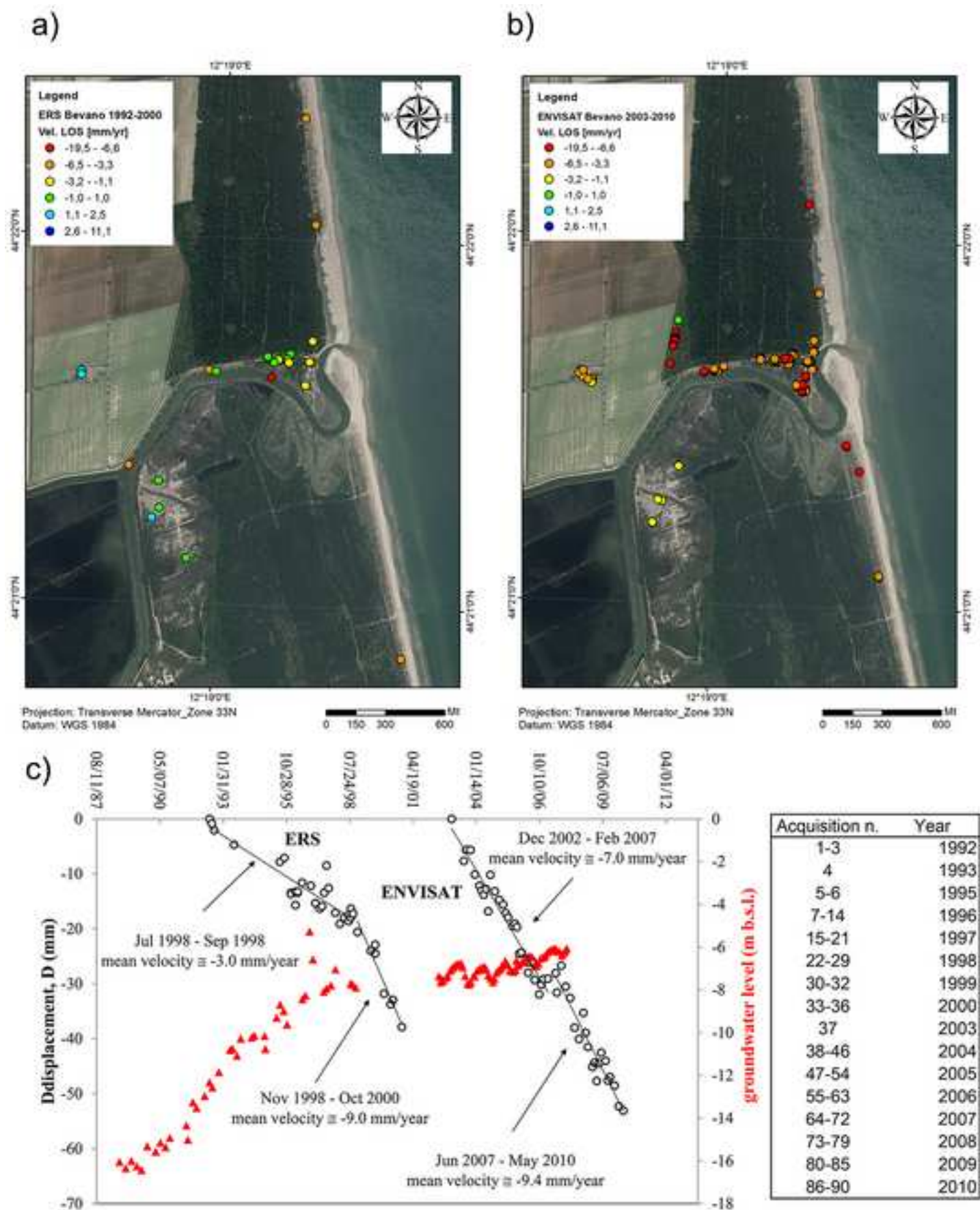


Figure5

[Click here to download high resolution image](#)

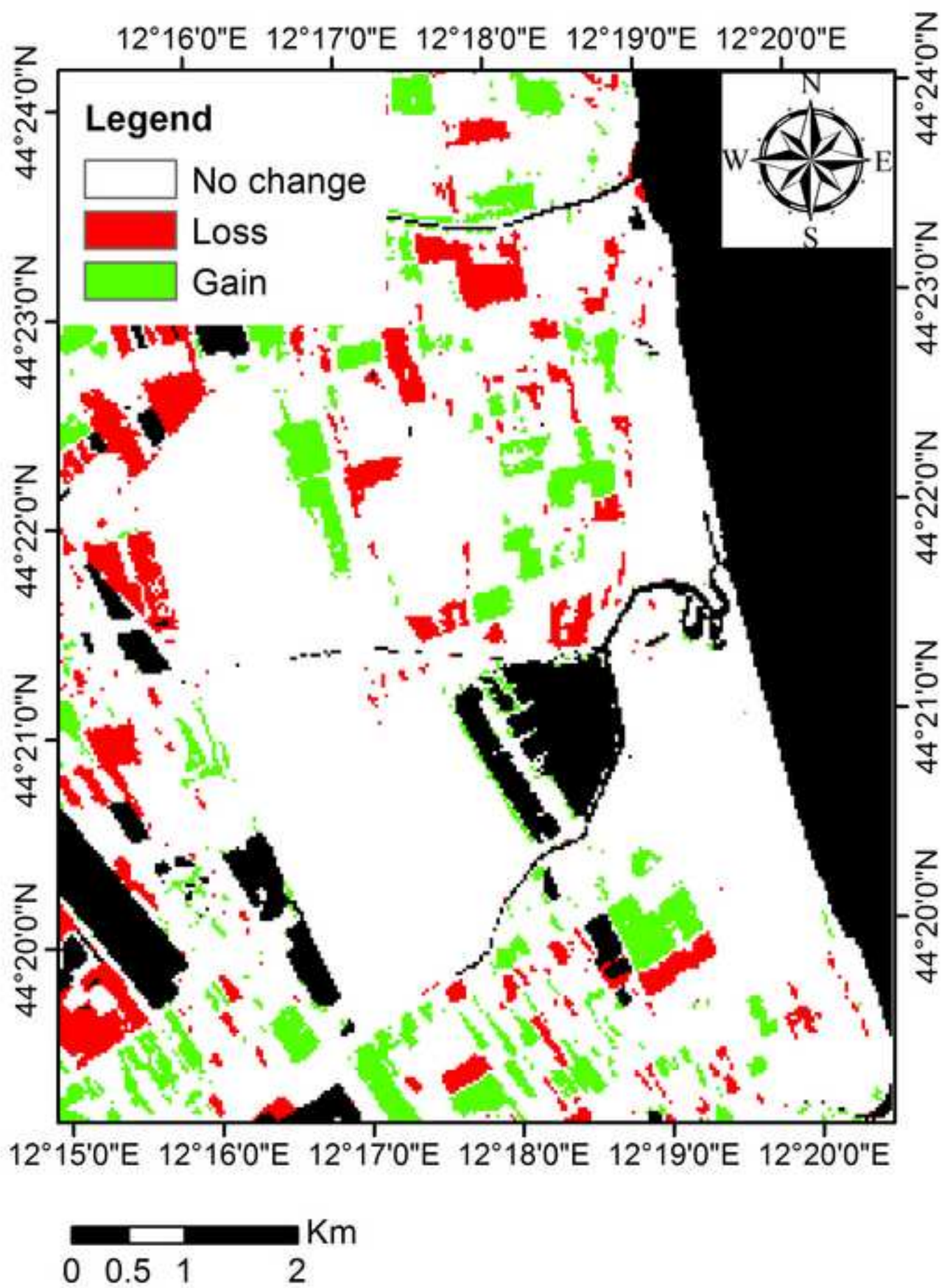


Figure6
[Click here to download high resolution image](#)

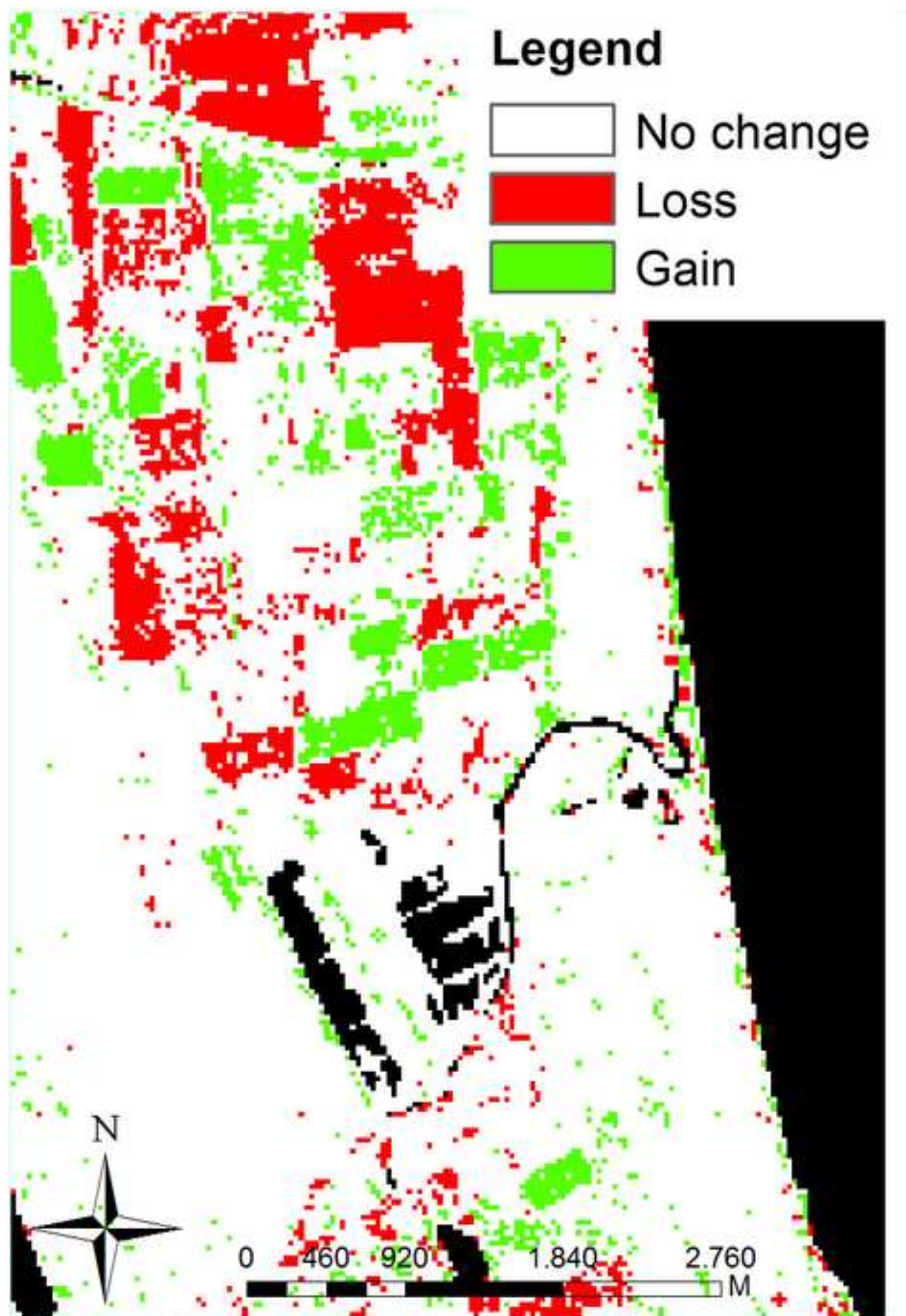


Figure7

[Click here to download high resolution image](#)

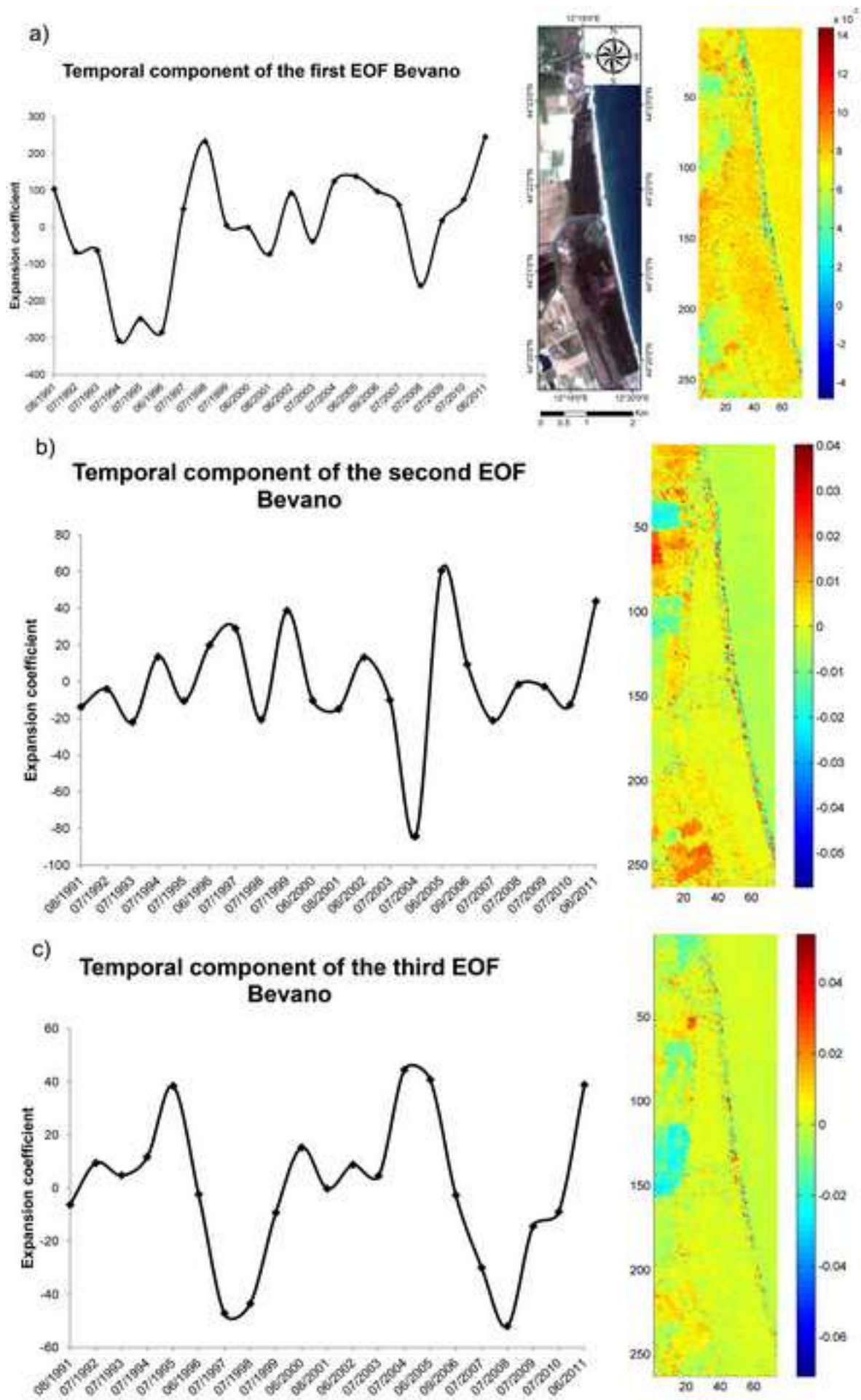


Figure8

[Click here to download high resolution image](#)

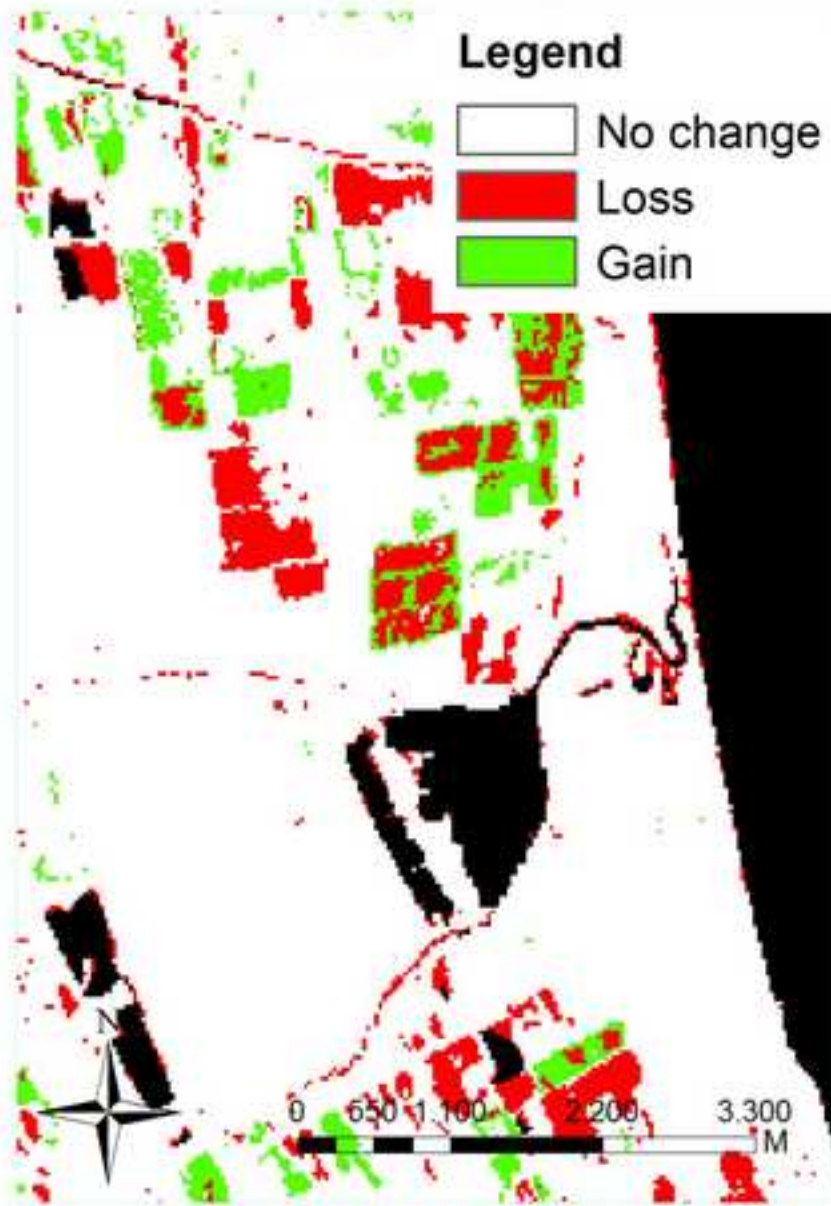


Figure9
[Click here to download high resolution image](#)

